

FIGGS: Faint Irregular Galaxies GMRT Survey – Overview, observations and first results

Ayesha Begum^{1*}, Jayaram N. Chengalur², I. D. Karachentsev³, M. E. Sharina³
and S. S. Kaisin³

¹*Institute of Astronomy, University of Cambridge, Madingley Road, Cambridge, CB3 0HA, UK*

²*National Centre for Radio Astrophysics, Post Bag 3, Ganeshkhind, Pune 411 007, India*

³*Special Astrophysical Observatory, Nizhni Arkhys 369167, Russia*

ABSTRACT

The Faint Irregular Galaxies GMRT Survey (FIGGS) is a Giant Metrewave Radio Telescope (GMRT) based HI imaging survey of a systematically selected sample of extremely faint nearby dwarf irregular galaxies. The primary goal of FIGGS is to provide a comprehensive and statistically robust characterization of the neutral inter-stellar medium properties of faint, gas rich dwarf galaxies. The FIGGS galaxies represent the extremely low-mass end of the dwarf irregular galaxies population, with a median $M_B \sim -13.0$ and median HI mass of $\sim 3 \times 10^7 M_\odot$, extending the baseline in mass and luminosity space for a comparative study of galaxy properties. The HI data is supplemented with observations at other wavelengths. In addition, distances accurate to $\sim 10\%$ are available for most of the sample galaxies. This paper gives an introduction to FIGGS, describe the GMRT observations and presents the first results from the HI observations. From the FIGGS data we confirm the trend of increasing HI to optical diameter ratio with decreasing optical luminosity; the median ratio of D_{HI}/D_{Ho} for the FIGGS sample is 2.4. Further, on comparing our data with aperture synthesis surveys of bright spirals, we find at best marginal evidence for a decrease in average surface density with decreasing HI mass. To a good approximation the disks of gas rich galaxies, ranging over 3 orders of magnitude in HI mass, can be described as being drawn from a family with constant HI surface density.

Key words: galaxies: dwarf – galaxies: kinematics and dynamics – radio lines: galaxies

1 INTRODUCTION

HI 21cm aperture synthesis observations of nearby spiral galaxies is a mature field with over three decades of history – probably something of the order of a thousand galaxies have already been imaged. However observers have tended to focus on bright ($\sim L_*$) galaxies with HI masses $\gtrsim 10^9 M_\odot$. HI observations of faint dwarf galaxies ($M_B \gtrsim -17$) generally require comparatively long integration times, and such galaxies have hence not been studied in similar numbers. While there have been some systematic HI surveys of dwarf galaxies (Swaters 1999; Stil & Israel 2002), these have generally been restricted to the brighter ($M_B \lesssim -14$) dwarfs.

In hierarchical models of galaxy formation, nearby dwarf galaxies would, in some ways, be analogs of the primordial building blocks of large galaxies. A systematic HI survey of the faintest dwarf galaxies could provide data that would be useful for a di-

verse range of studies, ranging from, for example, testing the predictions of cold dark matter models (e.g. Simon & Geha (2007); Blanton et al. (2007)), checking if such systems could be the host population of quasar absorption line systems (e.g. Zwaan et al. (2005); Kanekar & Chengalur (2005)) etc. As the most chemically unevolved systems in the present-day galaxy population, the faintest dwarfs provide unique laboratories for understanding star formation and galaxy evolution in extreme environments, i.e. low metallicity, low dust content, low pressure, low shear, and low escape velocity (e.g. Ekta et al. (2006)).

In this paper we describe and present the first results from a Giant Meterwave Radio Telescope (GMRT) based HI imaging study of faint dwarf galaxies – the Faint Irregular Galaxies GMRT Survey (FIGGS). The primary goal of FIGGS is to obtain high quality observations of the atomic ISM for a large, systematically selected sample of faint, gas rich, dwarf irregular (dIrr) galaxies. Our GMRT HI images are supplemented by single dish HI observations, HST V and I band images and ground based $H\alpha$ images

* E-mail:ayesha@ast.cam.ac.uk

from the 6-m BTA telescope. Additionally, the HII region abundances and H α rotation curves are being obtained on the William Herschel Telescope (WHT), Isaac Newton Telescope (INT) telescopes on La Palma and 6-m Russian BTA telescope, respectively.

This paper is organised as follows. In Section 2 we describe the design and the properties of the galaxy sample. The main science drivers for FIGGS are described in Section.3. The GMRT observations are described in Section 4 and the results of the survey are presented and discussed in Section 5.

2 FIGGS: SAMPLE DEFINITION AND PROPERTIES

The Faint Irregular Galaxies GMRT Survey – FIGGS, is a large observing program aimed at providing a comprehensive and statistically robust characterisation of the neutral ISM properties of faint, gas rich, dwarf irregular galaxies using the Giant Metrewave Radio Telescope (GMRT). The FIGGS sample forms a subsample of the Karachentsev et al.(2004) catalog of galaxies within ~ 10 Mpc. Specifically, the FIGGS sample consists of 65 faint dwarf irregular (dIrr)galaxies with:

- (i) absolute blue magnitude, $M_B \lesssim -14.5$,
- (ii) HI flux integral $> 1 \text{ Jy kms}^{-1}$
- (iii) optical B band major axis $\gtrsim 1.0$ arcmin.

The sample choice was dictated by a balance between achieving the scientific goals described in Section.3 and the practical limitations of the observing time. We note that the above mentioned criterion on the optical B band major axis was not strictly followed in few cases. Some unusual, very faint dwarf galaxies, with optical B band major axis < 1 arcmin were still included in our sample, as they are interesting cases to study in detail in HI. Further, for some of the galaxies in the FIGGS sample, fresh estimates of the distance (obtained after our observations were complete) imply absolute magnitudes slightly larger than the cut off above. These galaxies have however been retained in the sample. Some properties (mainly derived from optical observations) of galaxies in the FIGGS sample are listed in Table 1. The columns are as follows: Column(1) the galaxy name, Column(2)&(3) the equatorial coordinates (J2000), Column(4) the absolute blue magnitude (corrected for galactic extinction), Column(5) the Holmberg diameter in arcmin, Column(6) the (B-V) colour, Column(7) the distance in Mpc, Column(8) the method used to measure the distance – from the tip of the red giant branch (rgb), from membership in a group with known distance (grp), from the Tully-Fisher relation (tf), and from the Hubble flow (h). Column(9) gives the group membership of the galaxy, Column(10) the inclination determined from optical photometry (and assuming an intrinsic thickness, $q_o=0.2$) and Column(11) the reference for the (B-V) colour, and/or revised distance. The data presented in the Table 1 (except for the colour) is taken from Karachentsev et al. (2004) catalog, except that revised distances have been adopted, if available. As can be seen from the Table 1, tip of the red giant branch (rgb) distances (which are generally accurate to $\sim 10\%$) are available for most of the galaxies in our sample.

Figure 1 shows the histogram of the absolute blue magnitude (M_B), distance, HI mass, and HI mass to light ratio (M_{HI}/L_B) for the FIGGS sample, while Figure 2 compares the distributions of gas fraction, luminosity and dynamical mass of the FIGGS galaxies with that of existing samples of galaxies with HI aperture synthesis observations. The gas fraction and the dynamical masses for the FIGGS sample have been derived from the GMRT observations.

The FIGGS sample has a median $M_B \sim -13$ and a median HI mass $\sim 3 \times 10^7 M_\odot$, while spanning range of more than 100 in stellar light, gas mass and dynamical mass, and more than 4 in gas fraction. It can also be clearly seen that by focusing on fainter, lower mass galaxies than those observed in previous HI imaging studies, FIGGS bridges the transition to rotation dominated low mass spirals and provides a substantially extended baseline in mass and luminosity space for a comparative study of galaxy properties.

3 SCIENCE DRIVERS FOR FIGGS

The aim of FIGGS is to provide a large multi-wavelength database for a systematically selected sample of extremely faint dwarf irregular galaxies. As mentioned in Section 1, such a database could be used to address a diverse range of astrophysical questions. Rather than attempting to enumerate all of these, in this section, we describe in some detail a couple of key science drivers for the FIGGS survey.

3.1 Star formation and feedback in small galaxies

One of the main goals of FIGGS is to use the HI interferometric images in conjunction with the optical data to study the interplay between the neutral ISM and star formation in the faintest, lowest mass, gas rich dIrr galaxies. The gravitational binding energy for very faint dwarf irregular galaxies is not much larger than the energy output from a few supernovae; consequently star formation in such galaxies could have a profound effect on the morphology and kinematics of the ISM of these systems. The FIGGS data will enable us to study the ISM of most of our sample galaxies at a linear resolution of $\sim 15 - 300$ pc – i.e. comparable to the scales at which energy is injected into the ISM through supernova and stellar winds. FIGGS thus provide a unique opportunity to study the effects of feedback from star formation in low mass, gas rich galaxies, which in turn will allow us to understand the processes driving the evolution of these galaxies. For example, it has been suggested that star formation in dwarf galaxies occurs only above a constant threshold HI column density of $N_{HI} \sim 10^{21} \text{ cm}^{-2}$ (e.g. Skillman 1987; Taylor 1994). Such a threshold could be a consequence of disk dynamics (e.g. related to Toomre’s instability criterion; Kennicutt (1989)) or a consequence of some other physical process, e.g. self shielding or thermo-gravitational instability (Schaye (2004)). A preliminary study of a small subsample of FIGGS (Begum et al. (2006)) suggested that unlike brighter dwarfs, the faintest dwarf galaxies do not show well defined threshold density. A detailed comparison of H α and UV images with HI column density maps for the FIGGS sample will allow us to definitively answer the issue of the existence of a threshold density in the faintest galaxies and also to check whether the recipes for star formation derived from larger galaxies (Kennicutt (1989)) continue to be valid at this mass regime. These are critical issues in hierarchical galaxy formation models.

3.2 Dark and visible matter in small galaxies

The second major aim of this survey is to study the relation between dark and baryonic matter in the smallest known star forming galaxies. According to several models of galaxy formation and evolution, the first burst of star formation in dwarf galaxies below a critical halo circular velocity ($\sim 100 \text{ kms}^{-1}$) could lead to the loss of a significant fraction of baryons (e.g. Efstathiou 2000;

Table 1. The FIGGS sample

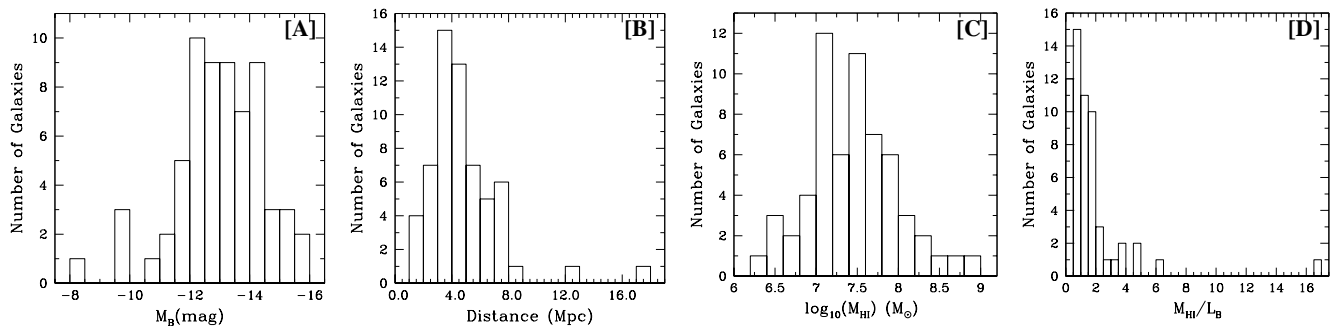
Galaxy	α (J2000) (h m s)	δ (J2000) ($^{\circ}$ ' ")	M_B (mag)	$D_{H\alpha}$ (')	B-V (mag)	Dist (Mpc)	D estm	Group	i_{opt} (deg)	Ref
SC 24	00 36 38.00	- 32 34 28	-8.39	0.6	-	1.66	Sculptor grp(?)	distant Irr	57	
And IV	00 42 32.30	+40 34 19	-12.23	1.1	0.47	6.3	rgb	Field	41	18,19
DDO 226	00 43 03.80	-22 15 01	-14.17	3.2	0.4	4.9	rgb	Sculptor	72	1
DDO 6	00 49 49.30	-21 00 58	-12.5	2.1	0.32	3.34	rgb	Sculptor	69	1
UGC 685	01 07 22.30	+16 41 02	-14.31	2.2	0.52	4.5	rgb	Field	46	1
KKH 6	01 34 51.60	+52 5 30	-12.42	0.9	0.43	3.73	rgb	IC 342/Maffei	55	13,17
KK 14	01 44 42.70	+27 17 16	-12.13	1.6	0.42	7.2	N672 grp	N672	71	13
KKH 11	02 24 35.00	+56 0 42	-13.35	1.7	-	3.0	Maffei grp	IC 342/Maffei	59	
KKH 12	02 27 27.00	+57 29 16	-13.03	2.2	-	3.0	Maffei grp	IC 342/Maffei	78	
KK 41	04 25 15.60	+72 48 21	-14.06	2.6	0.63	3.9	rgb	IC 342	57	2
UGCA 92	04 32 00.30	+63 36 50	-15.65	2.0	1.1	3.01	rgb	IC 342/Maffei	62	3, 17
KK 44	04 53 06.90	+67 05 57	-11.85	1.4	0.58	3.34	rgb	IC432	62	4
KKH 34	05 59 41.20	+73 25 39	-12.30	1.0	0.4	4.6	rgb	M81	58	13
E490-17	06 37 56.60	-25 59 59	-14.46	2.0	0.51	4.2	rgb	Field	42	5
HIZSS003	07 00 29.30	-04 12 30	-12.6	2.0	-	1.69	rgb	Field	55	
UGC 3755	07 13 51.80	+10 31 19	-14.90	1.8	0.55	6.96	rgb	Field	55	6,15
DDO 43	07 28 17.20	+40 46 13	-14.75	1.8	0.31	7.8	rgb	Field	48	7
KK 65	07 42 31.20	+16 33 40	-14.29	0.9	0.54	7.62	rgb	Field	58	8
UGC 4115	07 57 01.80	+14 23 27	-14.27	1.5	0.47	7.5	rgb	Field	58	13
KDG 52	08 32 56.00	+71 01 46	-11.49	1.3	0.24	3.55	rgb	M81	24	4
UGC 4459	08 34 06.50	+66 10 45	-13.37	1.6	0.45	3.56	rgb	M81	30	4
KK 69	08 52 50.70	+33 47 52	-12.76	2.0	-	7.7	N2683 grp	N2638	42	
UGC 5186	09 42 59.80	+33 15 52	-12.98	1.3	0.49	6.9	h	Field	83	13
UGC 5209	09 45 04.20	+32 14 18	-13.15	0.9	0.56	6.7	h	Field	17	8
UGC 5456	10 07 19.70	+10 21 44	-15.08	1.9	0.33	5.6	rgb	Field	62	9
HS 117	10 21 25.20	+71 06 58	-11.83	1.5	-	3.96	rgb	Field	55	
UGC 6145	11 05 35.00	-01 51 49	-13.14	1.7*	-	7.4	h	Field	64	
UGC 6456	11 28 00.60	+78 59 29	-14.03	1.5*	0.38	4.3	rgb	M81	60	11
UGC 6541	11 33 29.10	+49 14 17	-13.71	1.6	0.41	3.9	rgb	CVn I	57	10
NGC 3741	11 36 06.40	+45 17 7	-13.13	1.7	0.37	3.0	rgb	CVn I	58	7
KK 109	11 47 11.20	+43 40 19	-9.73	0.6	0.36	4.5	rgb	CVn I	49	13
DDO 99	11 50 53.00	+38 52 50	-13.52	3.5	0.38	2.6	rgb	CVn I	71	13
E379-07	11 54 43.00	-33 33 29	-12.31	1.1	0.23	5.2	rgb	Cen A	44	13
KK 127	12 13 22.70	+29 55 18	-15.30	1.0	0.4	13.0	ComaI grp	ComaI	69	17
E321-014	12 13 49.60	-38 13 53	-12.70	1.4	0.41	3.2	rgb	Cen A	67	13
UGC 7242	12 14 07.40	+66 05 32	-14.06	1.9	0.4	5.4	rgb	M81	68	13,17
CGCG 269-049	12 15 46.70	+52 23 15	-13.25	1.8	0.4	4.9	rgb	CVn I	77	16
UGC 7298	12 16 28.60	+52 13 38	-12.27	1.1	0.29	4.21	rgb	CVn I	58	4
UGC 7505	12 25 17.90	+26 42 53	-15.55	1.0	0.45	12.8	tf	ComaI	84	6
KK 144	12 25 27.90	+28 28 57	-12.59	1.5	0.4	6.3	h	CVn I	74	13
DDO 125	12 27 41.80	+43 29 38	-14.16	4.2	0.59	2.5	rgb	CVn I	58	6
UGC 7605	12 28 39.00	+35 43 05	-13.53	2.2	0.41	4.43	rgb	CVn I	44	13
UGC 8055	12 56 04.00	+03 48 41	-15.49	1.4	0.24	17.4	tf	Field	40	9
GR 8	12 58 40.40	+14 13 03	-12.11	2.2	0.32	2.1	rgb	Field	25	4
UGC 8215	13 08 03.60	+46 49 41	-12.26	1.0	0.38	4.5	rgb	CVn I	47	12, 17
DDO 167	13 13 22.80	+46 19 11	-12.70	1.6	0.32	4.2	rgb	CVn I	58	12
KK 195	13 21 08.20	-31 31 45	-11.76	1.3	-	5.22	rgb	M83	65	
KK 200	13 24 36.00	-30 58 20	-11.96	1.3	0.4	4.6	rgb	M83	53	13
UGC 8508	13 30 44.40	+54 54 36	-12.98	2.0	0.45	2.6	rgb	CVn I	55	6
E444-78	13 36 30.80	-29 14 11	-13.3	1.2*	0.49	5.25	rgb	M83	68	13
UGC 8638	13 39 19.40	+24 46 33	-13.68	1.2	0.51	4.27	rgb	CVn I	49	13, 17
DDO 181	13 39 53.80	+40 44 21	-13.03	1.6	0.46	3.1	rgb	CVn I	57	13
I4316	13 40 18.10	-28 53 40	-13.90	1.6	-	4.4	rgb	M83	52	
DDO 183	13 50 51.10	+38 01 16	-13.17	1.7	0.31	3.24	rgb	CVn I	75	9
UGC 8833	13 54 48.70	+35 50 15	-12.42	1.3	0.42	3.2	rgb	CVn I	28	13
KK 230	14 07 10.70	+35 03 37	-9.55	1.7	0.4	1.9	rgb	Field	35	4
DDO 187	14 15 56.50	+23 03 19	-12.51	2.28	0.28	2.5	rgb	Field	42	1
P51659	14 28 03.70	-46 18 06	-11.83	2.4*	-	3.6	rgb	Cen A	71	
KKR 25	16 13 47.60	+54 22 16	-9.96	1.2	-	1.86	rgb	Field	55	
KK 246	20 03 57.40	-31 40 54	-13.69	1.3	0.58	7.83	rgb	Field	68	13, 17

 *: Optical diameter measured at 25.0 mag arcsec⁻².

Table 1. (continued) The FIGGS sample

Galaxy	α (J2000) (h m s)	δ (J2000) ($^{\circ}$ ' ")	M_B (mag)	D_{HI} ($'$)	B-V (mag)	Dist (Mpc)	D estm	Group	i_{opt} (deg)	Ref
KK 250, UGC11583	20 30 15.30	+60 26 25	-14.54	1.8	0.91	5.6	N6946 grp	N6946	62	14
KK 251	20 30 32.60	+60 21 13	-13.72	1.6	0.37	5.6	N6946 grp	N6946	66	14
DDO 210	20 46 53.00	-12 50 57	-11.09	3.6	0.24	1.0	rgb	Field	62	4
UGCA 438	23 26 27.50	-32 23 26	-12.94	2.4	0.42	2.2	rgb	Sculptor	38	13
KKH 98	23 45 34.00	+38 43 4	-10.78	1.1	0.21	2.5	rgb	Field	58	13

References: 1-van Zee (2000) 2-Karachentsev et al. (1999) 3-Karachentsev et al. (1996) 4-Begum et al. (2006) 5-Parodi (2002) 6-Makarova (1999) 7-Taylor et al. (2005) 8-Makarova et al. (2002) 9-Hunter & Elmegreen (2006) 10-Bremnes et al. (2000) 11-Hopp & Schulte-Ladbeck (1995) 12-Bremnes et al. (1999) 13-Sharina et al. 2008 (in preparation) 14-Begum & Chengalur (2004b) 15-Tully et al. (2006) 16-Corbin et al. (2008) 17-Karachentsev et al. (2006) 18-Ferguson et al. (2000) 19-Chengalur et al. 2008 (in preparation)

**Figure 1.** The histogram of M_B (panel [A]), distance (panel [B]), logarithm of the HI mass (panel [C]) and the HI mass to light ratio, M_{HI}/L_B (panel [D]) for the FIGGS sample.

Dekel & Woo 2003). In fact, expulsion of gas because of energy input from supernovae has been postulated as a possible mechanism to produce dwarf elliptical galaxies from gas rich progenitors (e.g. Miralda-Escude & Rees (1997)). Although a complete expulsion of the ISM from galaxies has not been observed so far, expansive outward motions of the neutral gas in dwarf galaxies has been observed in at least two galaxies (viz. GR8, Begum & Chengalur 2003; NGC 625, Cannon et al. 2004). To test these models, high spatial resolution interferometric observations are crucial.

The Tully-Fisher (TF) relation demonstrates the existence of a tight relation between dark and luminous matter in bright spiral galaxies. Mcgaugh et al. (2000) (see also McGaugh (2005)) showed that dwarf galaxies deviate from the TF relation defined by bright spirals, but that the relationship is restored if one works with the total baryonic mass instead of the luminosity, i.e. a ‘‘Baryonic Tully Fisher’’ (BTF) relation. The FIGGS sample, both because it extends well beyond the region of rotation dominated dwarfs and because accurate distances are known for a large subsample, forms a very interesting dataset for studying TF and BTF relations. Most of the past studies have been done using the HI global velocity widths from the single dish observations (Geha et al. 2006; Mcgaugh et al. 2000). While for the brighter galaxies W_{20} (the velocity width at 20% emission, after correction for random motions and instrumental broadening), is a good measure of the rotational velocity of the galaxy (Verheijen & Sancisi 2001); it is unclear if this would remain true in the case of faint dwarf galaxies, where random motions could be comparable to the peak rotational velocities (e.g. Begum et al. 2003; Begum & Chengalur 2004a). For such galaxies, it is important to accurately correct for the pressure support (‘‘asymmetric drift’’ correction) for which one needs to know

both the rotation curve as well as the distribution of the HI gas, both of which can only be obtained by interferometric observations such as in FIGGS. The FIGGS sample would thus allow us to concretely answer this question using actual observational data.

The HI kinematics of FIGGS galaxies, in conjunction with the $H\alpha$ rotation curves can be used to accurately determine the density distribution of the dark matter halos of faint galaxies. Since stars generally make a minor contribution to the total mass in the FIGGS galaxies, accurate kinematical studies can provide direct information on the density profiles of their dark matter halos with less uncertainties arising from the unknown stellar mass to light ratio. Cosmological simulations of hierarchical galaxy formation predict a ‘‘universal’’ cusped density core for the dark matter halos of galaxies (e.g. Navarro et al. 2004). On the other hand, observations of dIrr galaxies indicate a constant density core for their dark matter halos (e.g. Weldrake et al. 2003; de Blok et al. 2003); however this comparison remains controversial (e.g. van den Bosch & Swaters 2001; de Blok 2005). FIGGS would not only provide a large sample for such a comparison, but would also provide a data set that is less subject to uncertainties due to the unknown stellar mass to light ratio or large scale non circular motions due to bars or spiral arms.

4 HI OBSERVATIONS AND DATA ANALYSIS

For all the GMRT HI observations, the observing bandwidth of 1 MHz was divided into 128 spectral channels, yielding a spectral resolution of 7.81 kHz (velocity resolution of 1.65 km s^{-1}). It is worth noting that this velocity resolution is ~ 4 times bet-

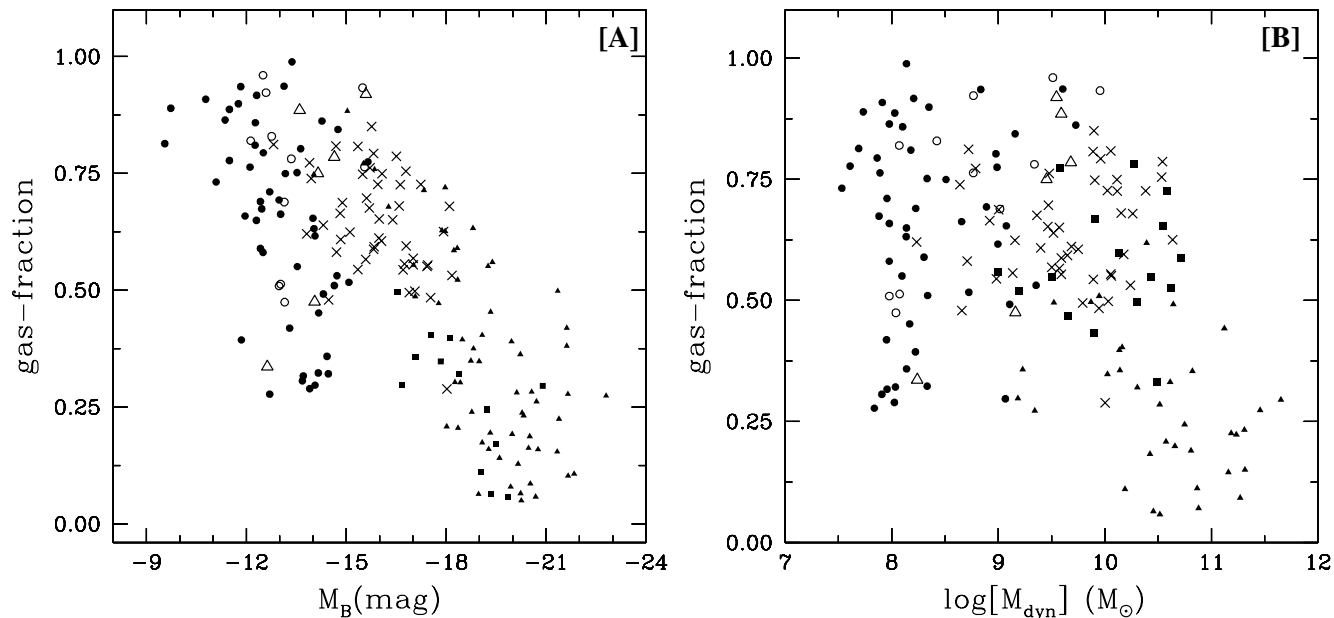


Figure 2. The gas fraction of FIGGS galaxies (circles) plotted as a function of the absolute blue magnitude (left) and dynamical mass (right). FIGGS galaxies with TRGB distances are shown as solid circles, whereas the remaining FIGGS galaxies are shown as empty circles. The same quantity is also plotted for the galaxies in literature with interferometric HI maps. The gas fraction (f_{gas}) is defined as $f_{\text{gas}} = M_{\text{gas}} / (M_{\text{gas}} + M_{\star})$. M_{gas} , is computed by scaling the HI mass by 1.33 to account for the primordial He fraction. No correction is made for the molecular gas. To compute the stellar mass, M_{\star} , the stellar mass to light ratio in the B band (Γ_{\star}) was derived from the observed (B-V) colour, using from the galaxy evolution models of Bell et al. (2003) and assuming a “diet” Salpeter IMF. Solid triangles are from McGaugh(2005), solid squares from Verheijen(2001), crosses from Swaters (1999) and empty triangles from Côté et al.(2000). Note how the GMRT FIGGS sample extends the coverage of all three galaxy properties.

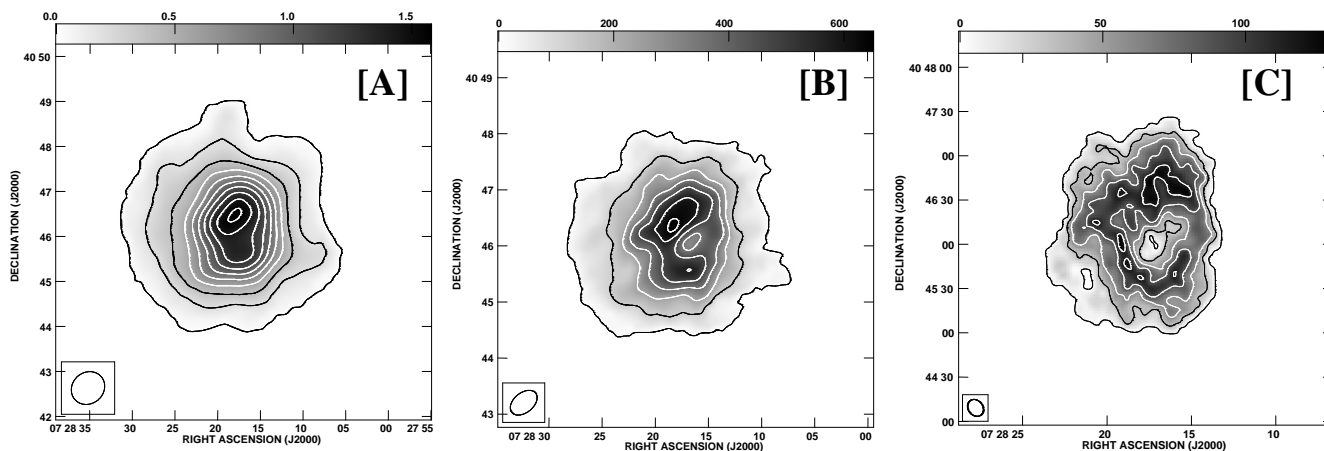


Figure 3. The figure shows the integrated HI emission from one of the galaxy in FIGGS sample, DDO 43 at various resolutions viz. $46'' \times 42''$ (panel [A]), $32'' \times 21''$ (panel [B]) and $15'' \times 12''$ (panel [C]). The first contour level and contour separation for these resolutions are (1.3,12.2), (2.5,18.1) and (4.0,26.2), respectively, in units of 10^{19} cm^{-2} .

ter than most earlier interferometric studies of such faint dwarf galaxies (e.g. Lo et al. (1993)). This high velocity resolution is crucial to detect large scale velocity gradients in the faintest dwarf galaxies (e.g. Begum et al. (2003); Begum & Chengalur (2004a)). For each observing run, absolute flux and bandpass calibration was done by observing one of the standard flux calibrators 3C48, 3C286

and 3C147, at the start and end of the observations. For the sample galaxies with low LSR velocities, particular care was taken to choose a bandpass calibrator which does not have any absorption feature in the relevant velocity range. The phase calibration was done once every 30 min by observing a nearby VLA phase calibrator source.

Table 2. Parameters of the GMRT observations

Galaxy	Date of Observations	Velocity Coverage (km s ⁻¹)	Time on Source (hours)	synthesised Beam (arcsec ²)	Noise (mJy)	Phase Cal	Cont Noise (mJy)
DDO 226	8 July 2004	257 – 469	3.5	52×46, 26×21, 19×17	3.2, 2.4, 2.1	0025-260	1.5, 0.9
DDO 6	1 Feb 2004	189 – 401	5.0	50×45, 26×21, 16×12	3.4, 1.7, 1.4	0116-208	1.3, 0.8
UGC 685	18 June 2004	51 – 263	3.5	42×40, 36×25, 27×19	4.0, 3.5, 3.1	0204+152	1.9, 1.0
KKH 6	9 July 2004	-45 – 166	4.0	41×33, 30×20, 16×11	3.0, 2.6, 2.2	0136+473	1.3, 0.8
KK 14	19 June 2004	317 – 529	5.0	41×38, 28×24, 16×13	3.0, 2.5, 2.1	3C48	1.6, 0.8
KKH 11	25 Nov 2004	205 – 415	3.0	46×36, 21×14, 13×10	3.0, 2.1, 1.8	0110+565	1.9, 0.9
KKH 12	16 July 2004	-36 – 176	3.7	47×37, 32×26, 16×11	1.6, 1.3, 1.0	0110+565	1.6, 0.8
UGCA 92	6 June 2005	-205 – 7	2.1	42×40, 26×21, 16×14	5.5, 4.2, 3.5	0410+769	2.9, 1.8
KK 41	8 July 2004	-152 – 60	3.0	53×52, 31×22, 20×16	1.9, 1.3, 1.1	0410+769	1.3, 0.8
KKH 34	9 June 2004	-5 – 216	4.5	53×50, 34×27, 22×18	4.0, 2.8, 2.4	0410+769	1.7, 0.9
E490-17	17 June 2004	404 – 616	3.5	49×46, 35×25, 24×14	6.0, 5.8, 4.0	0608-223	2.4, 1.2
UGC 3755	11 Jan 2004	209 – 421	5.0	42×40, 28×25, 18×16	3.8, 3.0, 2.6	0745+101	1.9, 1.0
DDO 43	16 Jan 2005	248 – 460	3.5	46×42, 32×21, 15×12	3.2, 2.6, 2.2	0713+438	1.6, 1.0
KK 65	25 Nov 2004	173 – 385	5.0	41×37, 27×25, 19×17	3.0, 2.3, 1.9	0738+177	1.7, 0.9
UGC 4115	10 July 2004	235 – 447	4.0	42×41, 34×26, 18×14	3.4, 3.2, 2.7	0745+101	1.8, 1.1
KK 69	3 Jan 2005	357 – 569	4.0	56×51, 42×35, 28×24	4.0, 3.0, 2.5	0741+312	1.9, 1.3
UGC 5186	26 Nov 2004	445 – 657	5.0	41×37, 27×24, 15×13	3.0, 2.2, 1.6	0958+324	1.5, 0.8
UGC 5209	15 Jan 2005	432 – 644	4.5	41×37, 27×24, 18×15	3.2, 2.6, 2.1	0958+324	1.6, 0.9
UGC 5456	9 July 2004	438 – 650	3.0	41×36, 34×25, 22×20	4.0, 3.2, 2.6	1008+075	1.9, 1.2
HS 117	8 Aug 2005	-143 – 69	3.0	46×42	3.8	1035+564	1.8, 1.1
UGC 6145	11 Feb 2005	634 – 846	5.0	42×37, 34×27, 20×14	2.4, 2.0, 1.8	1150-003	1.4, 1.0
UGC 6456	19 June 2004	-208 – 3	3.5	53×39, 23×20, 16×15	5.0, 3.4, 3.0	1435+760	2.0, 1.2
UGC 6541	29 Nov 2004	144 – 356	5.0	42×33, 28×23, 21×15	3.8, 3.0, 2.4	1035+564	2.2, 1.0
KK 109	6 June 2005	106 – 318	4.0	49×41, 27×21, 18×13	4.8, 3.5, 2.7	1227+365	2.3, 1.2
DDO 99	30 June 2005	136 – 348	3.5	45×37, 28×23, 19×16	3.8, 3.0, 2.7	1227+365	2.0, 1.1
E379-07	19 Jan 2005	534 – 746	4.5	54×47, 33×24, 19×18	3.0, 2.0, 1.7	1154-350	1.8, 1.1
KK 127	9 July 2004	46.0 – 258	3.5	49×44	3.0	1227+365	1.7, 1.1
E321-014	7 Oct 2005	507 – 719	3.5	51×45, 28×18, 15×10	3.9, 2.7, 2.3	1154-350	1.8, 0.9
UGC 7242	3 Feb 2004	-37 – 174	6.5	45×37, 27×23, 18×15	2.2, 1.9, 1.6	1313+675	1.4, 0.8
UGC 7505	28 Nov 2004	210 – 422	3.0	45×39, 28×27, 24×18	4.0, 3.2, 2.8	1227+365	1.6, 1.1
KK 144	12 July 2004	377 – 589	4.5	41×40, 28×24, 19×14	4.0, 3.2, 2.7	1221+282	1.8, 1.0
DDO 125	6 June 2005	89 – 301	4.0	45×36, 31×22, 20×14	4.2, 3.8, 3.0	1227+365	1.8, 1.2
UGC 7605	1 Feb 2004	204 – 416	7.0	43×38, 29×24, 16×12	2.3, 2.0, 1.7	1227+365	1.5, 0.9
UGC 8055	13 June 2005	512 – 724	6.0	40×37, 27×25, 19×17	3.3, 2.7, 2.4	1254+116	2.0, 1.2
UGC 8215	29 Nov 2004	112 – 324	6.0	46×39, 28×22, 17×14	3.6, 2.7, 2.4	1227+365	2.1, 1.2
DDO 167	10 July 2004	57 – 269	3.5	51×38, 29×23, 19×16	6.0, 4.7, 4.1	1227+365	2.5, 1.3
KK 195	4 Jan 2005	460 – 672	4.5	62×54, 30×24, 18×16	3.9, 2.7, 2.1	1018-317	2.2, 1.1
KK 200	26 Nov 2004	381 – 593	5.0	48×47, 32×23, 21×17	2.9, 2.1, 1.8	1316-336	1.8, 0.9
UGC 8508	31 Jan 2004	-44 – 167	7.0	42×38, 32×24, 18×15	2.6, 2.2, 1.8	1400+621	1.5, 0.8
E444-78	20 June 2004	475 – 686	2.5	48×47, 26×21, 18×11	6.0, 4.0, 3.5	1316-336	2.3, 1.6
UGC 8638	9 July 2004	168 – 380	2.5	44×36, 25×17, 16×11	4.0, 2.6, 2.0	1330+251	1.7, 1.0
DDO 181	6 June 2005	96 – 308	5.5	50×41, 26×21, 17×14	5.2, 3.4, 2.7	3C286	2.1, 1.2
I4316	7 Aug 2005	474 – 686	2.7	48×46, 26×20, 15×11	3.6, 2.8, 2.3	1316-336	1.9, 1.0
DDO 183	31 Jan 2004	86 – 298	6.5	42×38, 31×24, 17×13	2.7, 2.0, 1.7	1331+305	1.5, 0.9
UGC 8833	16 June 2004	121 – 333	3.5	41×39, 30×25, 21×18	3.7, 2.8, 2.3	3C286	2.0, 1.5
DDO 187	16 June 2004	47 – 259	2.5	46×37, 30×25, 19×13	5.0, 4.1, 3.4	3C286	2.4, 1.5
P51659	14 Jan 2005	285 – 497	3.0	48×41, 26×20, 15×14	3.4, 2.6, 2.2	1316-336	1.9, 1.1
KK 246	16 June 2004	255 – 469	2.5	61×39, 36×21, 15×11	4.2, 3.5, 2.9	1923-210	2.2, 1.2
KKH 98	10 July 2004	-243 – -32	6.0	42×41, 32×28, 15×14	3.2, 2.7, 2.4	0029+349	2.1, 1.2

The GMRT data were reduced in the usual way using the standard tasks in classic AIPS. For each run, bad visibility points were edited out, after which the data were calibrated. The GMRT does not do online doppler tracking – any required doppler shifts have to be applied during the offline analysis. However, for all of the sample galaxies, the differential doppler shift over our observing interval was much less than the channel width, hence, there was no need to apply any offline correction. The GMRT has a hybrid configuration (Swarup et al. 1991) with 14 of its 30 antennas located

in a central compact array with size ≈ 1 km (≈ 5 k λ at 21cm) and the remaining antennas distributed in a roughly “Y” shaped configuration, giving a maximum baseline length of ≈ 25 km (≈ 120 k λ at 21 cm). The baselines obtained from antennas in the central compact array are similar in length to those of the “D” array of the VLA, while the baselines between the arm antennas are comparable in length to the “B” array of the VLA. A single observation with the GMRT hence yields information on both large and small angular scales. Data cubes at a range of angular resolutions were made

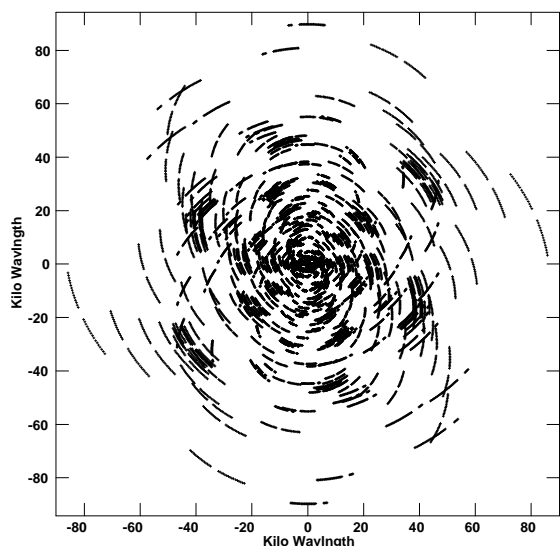


Figure 4. The figure shows the (u,v) coverage for UA 92, the sample galaxy with the shortest on source integration time (viz. 2.1 hours)

using appropriate (u,v) ranges and tapers. In this paper we present only the low resolution HI images, i.e. made using (u,v) ranges of $\sim 0-5$ k λ , $0-10$ k λ and $0-20$ k λ . Higher resolution observations of the FIGGS sample will be presented in the companion paper. To obtain the low resolution HI images for the sample galaxies, the uv -taper at each (u,v) range was adjusted to achieve as close as possible to a circular synthesized beam. A low resolution data cube was generated for each galaxy, using the AIPS task IMAGR, and the individual channels were inspected using the task TVMOVIE to identify the channels with HI emission. Emission was detected from all of the galaxies in our sample, except for SC 24, HS 117, KK 127 and KKR 25. Apart from HS 117, all of these galaxies were previously claimed to be detected by single dish observations. The GMRT data suggest that the previous flux measurements were spurious, probably as a result of confusion with galactic emission. The galaxies KK 127 and SC 24 are likely to be distant dwarf irregular galaxies whereas KKR 25 is a normal dwarf spheroidal galaxy (Begum & Chengalur (2005); Karachentsev et al. (2006)). In the case of HS 117, single dish observations did not detect this galaxy (Huchtmeier & Skillman (1998)). The HI data given in Karachentsev et al. (2002) is a result of misidentifying galactic HI emission as emission from HS 117. For the rest of the galaxies in the sample, frequency channels with emission were identified and the continuum maps were made at both low ($26'' \times 22''$) and high ($5'' \times 5''$) resolutions using the average of the remaining line free channels. No extended or compact emission was detected from the disk of any of our sample galaxies. All other continuum sources lying with the field of view were subtracted using the task UVSUB. After continuum subtraction, deconvolved data cubes of the line emission were made at a range of resolutions using the AIPS task IMAGR.

HI images at both high and low spatial resolutions are crucial for a complete understanding of the properties of the atomic ISM of faint dwarf galaxies. As an example, Figure 3 shows the integrated HI column distribution at various resolutions for one of the FIGGS galaxies DDO 43. This galaxy shows a faint, extended HI envelope which is only seen clearly in the lowest resolution HI maps. On the other hand, DDO 43 also has a large hole in the center (see also the

VLA observations in Simpson, Hunter, & Nordgren (2005)), which is seen in the high resolution HI map. However this hole in the HI distribution is not at all obvious in the low resolution HI maps due to the beam smearing.

The setup and observational results for 49 galaxies from the FIGGS sample are given in Table 2. For the remaining 15 sample galaxies, the details of the observations and data analysis can be found in Begum et al. 2003; Begum & Chengalur 2003, 2004a,b; Begum et al. 2005; Begum & Chengalur 2005; Begum et al. 2005, 2006 and Chengalur et al. 2008 (in preparation). In the case of UGCA 438, most of the short baselines were missing because of the non availability of some of the GMRT antennas during the observing run, thus missing the diffuse, extended emission from the galaxy. Future observations of this galaxy are planned. We have not considered this galaxy for the analysis in this paper. The columns in Table 2 are as follows: Column(1) the galaxy name, Column(2) the date of observations, Column(3) the velocity coverage of the observation, Column(4) the total integration time on source, Column(5) the synthesized beam sizes of the data cubes, Column(6) the rms noise per channel for the different resolution data cubes, Column(7) the phase calibrator used, Column(8) the 3σ limits on continuum emission from the galaxy at resolutions of ($26'' \times 22''$) and ($5'' \times 5''$) respectively. We note that although for some of the sample galaxies the on-source integration time is short ($\sim 2 - 2.5$ hours), the hybrid configuration of the GMRT leads to a reasonable sampling of the (u,v) plane. As an example, Figure 4 shows the (u,v) coverage for UA 92, the sample galaxy with the shortest on source integration time (viz. 2.1 hours).

We examined the line profiles at various locations in the galaxy and found that they were (to zeroth order) symmetric and single peaked. For some galaxies, in the very high column density regions, a double gaussian and/or a gauss-hermite fit does provide a somewhat better description of the data, but even in these regions, the mean velocity produced by the moment method agrees within the errors with the peak velocity of the profile. Since we are interested here mainly in the systematic velocities, moment maps provide an adequate description of the data. Moment maps (i.e. maps of the total integrated flux (moment 0), the flux weighted velocity (moment 1) and the flux weighted velocity dispersion (moment 2)) were made from the data cubes using the AIPS task MOMNT. To obtain the moment maps, lines of sight with a low signal to noise ratio were excluded by applying a cutoff at the 2σ level, (σ being the rms noise level in a line free channel), after smoothing in velocity (using boxcar smoothing three channels wide) and position (using a gaussian with full width at half maximum (FWHM) ~ 2 times that of the synthesized beam). Maps of the velocity field were also made in GIPSY using single gaussian fits to the individual profiles. The velocities produced by MOMNT in AIPS are in reasonable agreement with those obtained using a single gaussian fit. Note that the AIPS moment 2 map systematically underestimates the velocity dispersion (as obtained from gaussian fitting) particularly near the edges where the signal to noise ratio is low. This can be understood as the effect of the thresholding algorithm used by the MOMNT task to identify the regions with signal.

5 RESULTS AND DISCUSSION

A detailed analysis of FIGGS data will be presented in companion papers. Here we restrict ourselves to a preliminary analysis of the global HI and optical properties of the FIGGS sample.

The global HI profiles for our sample galaxies, obtained from

Table 3. Results from the GMRT observations

Galaxy	FI_{GMRT} (Jy kms^{-1})	V_{sys} (kms^{-1})	ΔV_{50} (kms^{-1})	D_{HI} (l)	M_{HI} ($10^6 M_{\odot}$)	$\frac{M_{HI}}{L_B}$	$\frac{D_{HI}}{D_{Ho}}$	$\frac{FI_{GMRT}}{FI_{SD}}$	i_{HI} (deg)	Ref
And IV	19.5 ± 2.0	237.0	90.0	7.6	205.19	16.9	6.9	0.87 ± 0.11	55.0 ± 5.0	14
DDO 226	4.8 ± 0.5	358.57	37.0	3.5	25.95	0.36	1.09	0.79 ± 0.10	55.0 ± 5.0	1
DDO 6	2.6 ± 0.3	291.83	19.2	3.3	6.82	0.44	1.57	0.77 ± 0.10	—	2
UGC 685	11.8 ± 1.2	156.29	64.4	3.6	56.15	0.68	1.64	0.99 ± 0.11	36.0 ± 4.0	3
KKH 6	3.0 ± 0.3	59.92	28.0	2.6	10.18	0.71	2.90	0.72	30.0 ± 3.0	2
KK 14	1.8 ± 0.2	420.11	27.7	2.4	21.93	1.98	1.50	0.89 ± 0.10	45.0 ± 3.0	6
KKH 11	25.0 ± 2.5	295.71	84.4	7.2	52.88	1.56	4.23	1.09 ± 0.12	66.0 ± 3.0	2
KKH 12	5.5 ± 0.6	70.0	48.4	4.6	11.63	0.46	2.10	0.34	60.0 ± 3.0	2
KK 41	18.8 ± 1.9	-54.2	38.5	8.7	67.20	1.03	3.35	0.42	30.0 ± 4.0	2
UGCA 92	70.0 ± 7.1	-94.58	56.2	9.0	156.05	0.55	4.50	0.70	56.0 ± 3.0	5
KK 44	4.6 ± 0.4	77.5	21.4	3.2	12.2	1.4	2.3	1.02 ± 0.11	61.0 ± 5.0	11
KKH 34	2.1 ± 0.2	106.29	21.7	2.6	10.44	0.81	2.60	0.89 ± 0.1	45.0 ± 3.0	2
E490-17	7.3 ± 0.7	505.17	39.2	3.0	30.26	0.32	1.50	1.11 ± 0.13	—	2
UGC 3755	6.5 ± 0.7	310.81	34.5	3.0	41.30	0.29	1.67	0.96 ± 0.11	46.0 ± 4.0	2
DDO 43	14.2 ± 1.4	352.63	36.5	5.0	203.02	1.64	2.78	1.20 ± 0.15	30.0 ± 5.0	2
KK 65	2.52 ± 0.3	281.45	33.3	2.1	34.38	0.43	2.33	0.97 ± 0.11	47.0 ± 4.0	2
UGC 4115	21.6 ± 2.2	342.78	78.0	6.0	285.53	3.59	4.00	1.00 ± 0.11	50.0 ± 7.0	2
KDG 52	3.8 ± 0.4	116.0	20.6	3.5	10.8	1.8	2.7	0.85 ± 0.11	23.0 ± 4.0	11
UGC 4459	21.5 ± 2.2	19.2	29.6	4.5	64.2	1.4	2.8	1.01 ± 0.11	30.0 ± 4.0	11
KK 69	3.0 ± 0.3	462.04	13.1	4.0	41.89	2.11	2.0	1.07 ± 0.12	35.0 ± 3.0	2
UGC 5186	1.4 ± 0.1	546.08	34.0	1.6	15.66	0.65	1.00	0.96 ± 0.11	—	2
UGC 5209	2.0 ± 0.2	535.19	31.6	1.9	21.10	0.75	2.11	1.21 ± 0.13	—	7
UGC 5456	8.0 ± 0.8	526.75	62.4	2.8	58.96	0.35	1.50	1.16 ± 0.14	60.0 ± 5.0	3
UGC 6145	2.1 ± 0.2	753.0	41.1	2.7	27.02	0.96	1.59	1.00 ± 0.11	55.0 ± 5.0	5
UGC 6456	10.1 ± 1.0	-93.69	37.4	3.7	43.89	0.69	2.47	0.72	65.0 ± 3.0	2
UGC 6541	2.7 ± 0.3	249.36	25.5	2.1	9.65	0.20	1.29	0.90 ± 0.10	—	2
NGC 3741	74.7 ± 7.5	228.8	83.4	14.6	130.0	4.7	8.80	—	68.0 ± 4.0	10
KK 109	0.76 ± 0.08	210.67	18.2	1.4	3.62	2.98	1.00	1.08 ± 0.12	—	2
DDO 99	33.0 ± 3.3	251.22	33.7	9.6	52.42	1.32	2.74	1.04 ± 0.12	—	5
E379-07	5.0 ± 0.5	644.04	28.5	3.6	31.77	2.43	3.27	0.93 ± 0.10	$31.0 - 6.0$	8
E321-014	1.3 ± 0.1	609.39	19.0	2.1	3.13	0.17	1.49	0.46 ± 0.05	—	5
UGC 7242	7.2 ± 0.7	66.05	66.5	4.0	45.75	0.70	2.11	1.02 ± 0.11	58.0 ± 3.0	5
CGCG 269-049	4.7 ± 0.5	159.0	26.6	2.6	26.4	0.9	2.3	0.91 ± 0.10	42.0 ± 4.0	11,12
UGC 7298	5.2 ± 0.5	174.0	21.4	3.5	21.6	1.7	3.1	1.06 ± 0.11	28.0 ± 3.0	11
UGC 7505	11.5 ± 1.2	316.0	125.1	5.3	442.78	1.72	5.30	0.92 ± 0.10	70.0 ± 4.0	5
KK 144	8.7 ± 0.9	479.54	37.5	4.7	81.15	4.80	3.13	1.01 ± 0.11	57.0 ± 4.0	2
DDO 125	21.7 ± 2.2	206.25	27.4	7.0	31.87	0.44	1.67	1.00 ± 0.11	—	5
UGC 7605	4.93 ± 0.5	309.95	25.8	3.3	22.29	0.55	1.50	0.87 ± 0.10	40.0 ± 5.0	2
UGC 8055	11.0 ± 1.1	609.05	85.6	4.2	782.64	3.20	3.00	1.34 ± 0.32	45.0 ± 3.0	3
GR 8	9.0 ± 0.9	217.0	26.0	4.3	10.38	1.02	2.3	1.03 ± 0.11	27.0 ± 4.0	11
UGC 8215	4.5 ± 0.5	224.15	24.6	3.5	21.41	1.72	3.50	1.05 ± 0.11	45.0 ± 4.0	2
DDO 167	3.7 ± 0.4	150.24	18.6	2.0	14.51	0.78	1.25	0.88 ± 0.10	—	4
KK 195	4.8 ± 0.5	571.91	24.0	5.0	30.50	3.88	3.85	0.91 ± 0.11	$52.0 - 4.0$	5
KK 200	1.6 ± 0.2	493.69	17.4	1.4	7.96	0.84	1.00	0.94 ± 0.11	—	2
UGC 8508	18.3 ± 1.8	56.17	45.8	6.6	29.07	1.21	3.30	1.21 ± 0.14	53.0 ± 4.0	4
E444-78	2.3 ± 0.2	577.0	30.6	0.9	14.62	0.45	1.67	0.83 ± 0.12	$42.0 - 3.0$	9
UGC 8638	3.5 ± 0.4	275.9	30.8	1.2	13.76	0.30	1.00	0.90 ± 0.10	—	2
DDO 181	12.2 ± 1.2	213.6	39.1	5.2	27.55	1.08	3.25	1.07 ± 0.12	53.0 ± 3.0	2
I4316	2.2 ± 0.2	576.34	21.5	2.8	10.01	0.18	1.00	1.05 ± 0.12	—	5
DDO 183	10.5 ± 1.1	188.37	28.7	4.6	25.90	0.90	2.71	1.07 ± 0.12	67.0 ± 3.0	2
UGC 8833	6.3 ± 0.6	221.03	27.8	3.0	15.16	1.05	2.31	1.05 ± 0.11	26.0 ± 3.0	2
KK 230	2.2 ± 0.2	63.31	17.0	3.0	1.90	1.9	3.3	0.86 ± 0.11	50.0 ± 4.0	11
DDO 187	11.1 ± 1.1	159.95	30.6	3.4	16.30	1.04	1.36	0.93 ± 0.10	37.0 ± 4.0	2
P51659	17.4 ± 1.7	391.48	46.4	6.5	52.99	6.31	2.71	1.03 ± 0.11	68.0 ± 4.0	5
KK 246	4.4 ± 0.4	434.71	52.2	3.5	84.50	1.36	2.69	0.53	56.0 ± 3.0	5
KK 250	16.4 ± 1.6	126.0	95.5	5.8	121.0	1.2	3.2	0.82 ± 0.11	73.0 ± 4.0	13
KK 251	10.6 ± 1.0	130.3	51.7	4.2	78.0	1.6	2.6	0.73 ± 0.11	59.0 ± 5.0	13
DDO 210	12.1 ± 1.2	-139.5	19.1	4.8	2.8	1.0	1.3	1.05 ± 0.11	26.0 ± 7.0	11
KKH 98	4.4 ± 0.4	-132.26	20.7	3.8	6.46	2.02	3.45	1.07 ± 0.12	46.0 ± 5.0	2

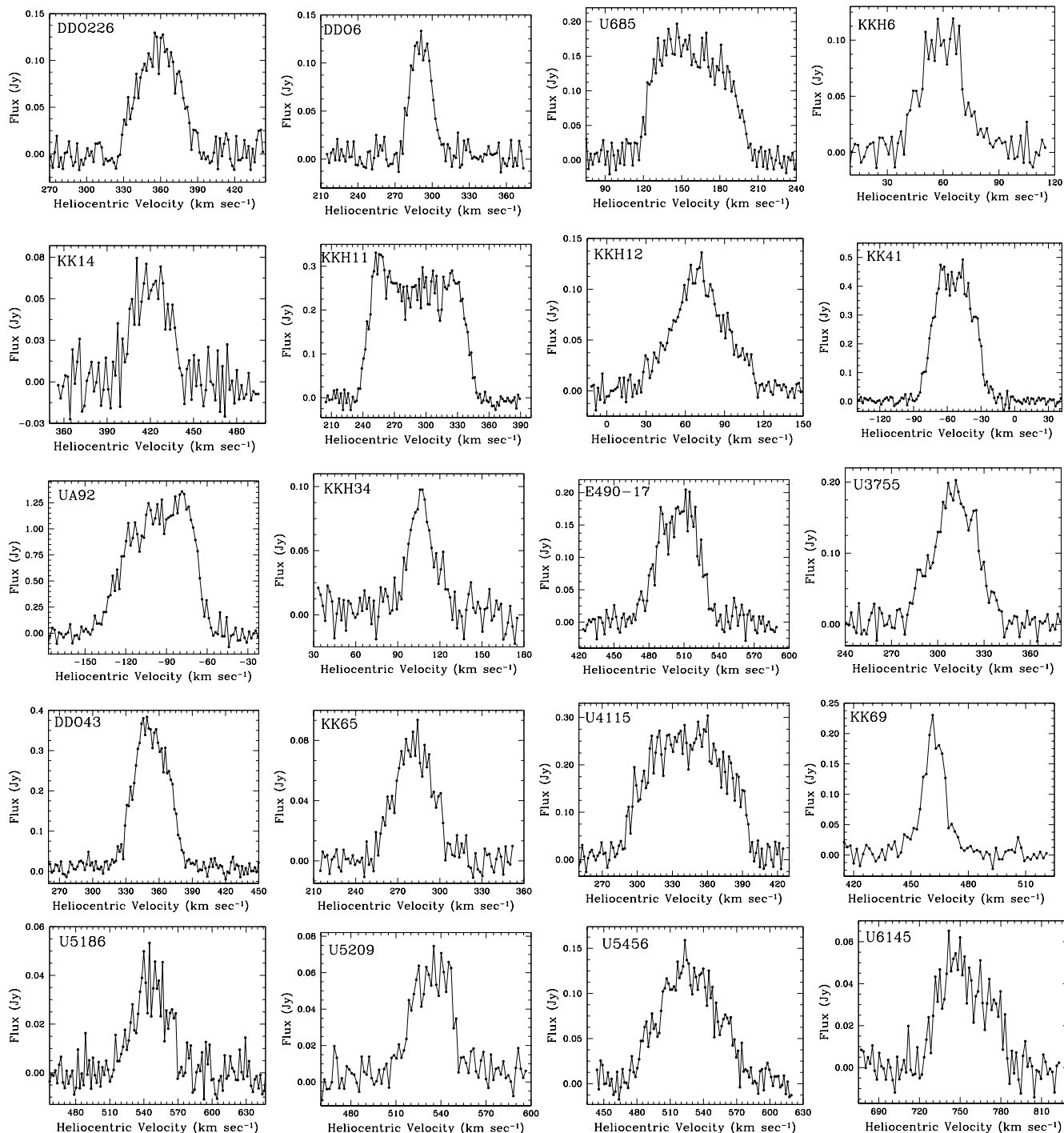


Figure 5. The global HI profiles of the sample galaxies obtained from the lowest resolution data cubes (see Table 2).

the coarsest resolution data cubes (see Table 2) are shown in Figure 5. The parameters derived from the global HI profiles for the whole FIGGS sample are listed in Table 3. The columns are as follows: (1) the galaxy name, (2) the integrated HI flux along with the errorbars, (3) the central heliocentric velocity (V_{sys}), (4) the velocity width at 50% of the peak (ΔV_{50}), (5) the HI diameter (in arcmin) at a column density of $\sim 10^{19}$ atoms cm^{-2} (D_{HI}), (6) the

derived HI mass (M_{HI}), (7) the HI mass-to-light ratio (M_{HI}/L_B), (8) the ratio of the HI diameter to the Holmberg diameter, (9) the ratio of the GMRT flux to the single dish flux ($F_{\text{I}}/F_{\text{I,SD}}$), (10) the inclination as measured from the HI moment 0 maps (i_{HI}), and (11) the reference for the single dish fluxes.

As seen in Column(9) in Table 3, the HI flux measured from the GMRT HI profiles for most FIGGS galaxies, in general, agree

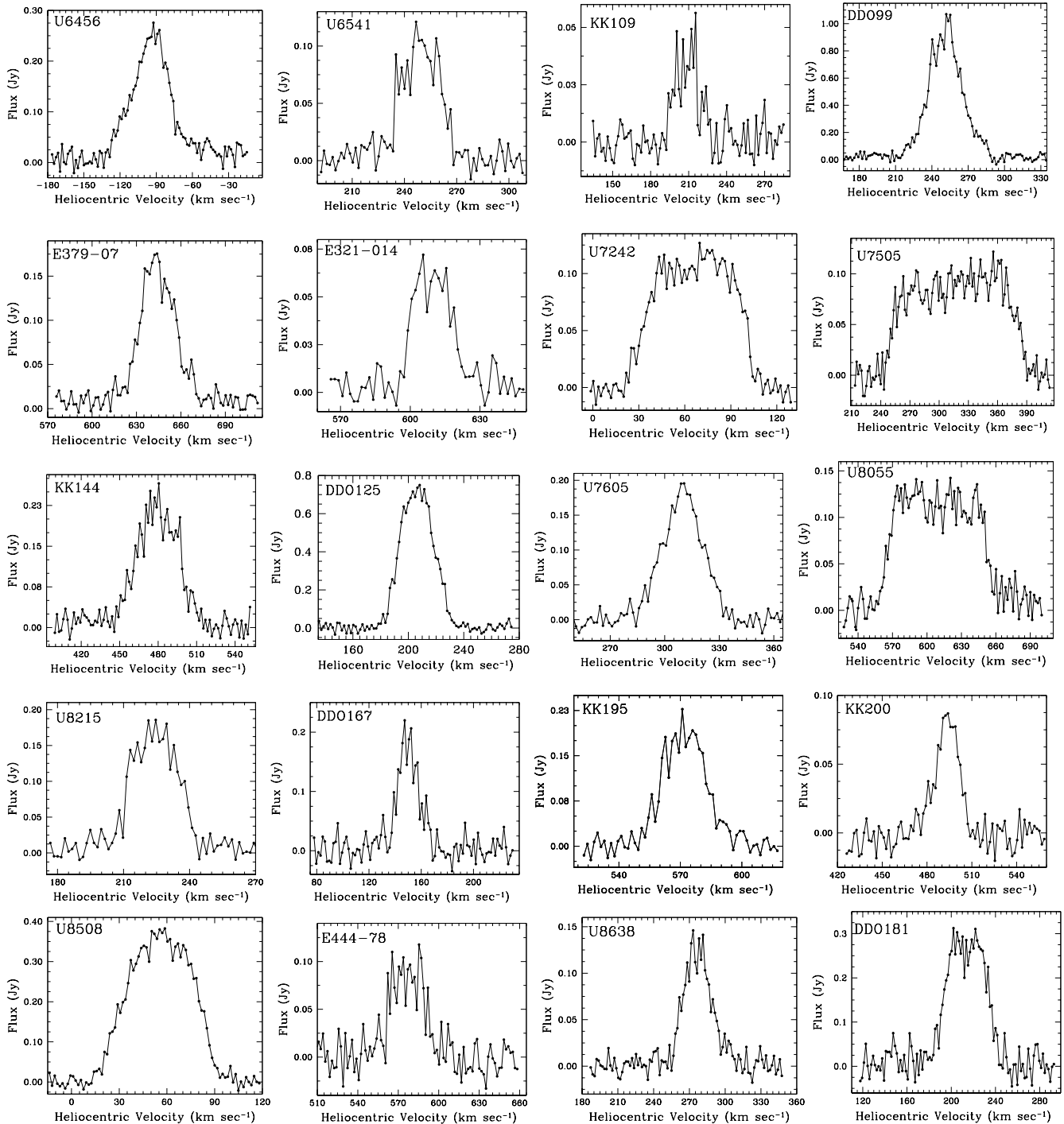


Figure 5. (continued) The global HI profiles of the sample galaxies obtained from the lowest resolution data cubes (see Table 2).

(within the errorbars) with the values obtained from the single dish observations. The average ratio of GMRT flux to single dish flux is 0.98. This indicates that in general no flux was missed because of the missing short spacings in our interferometric observations. However, for some galaxies the integrated flux derived from the GMRT observations is significantly smaller than the single dish values. The GMRT fluxes could be lower than those obtained from

single dish measurements either because of (i) a calibration error or (ii) a large fraction of HI being in an extended distribution that is resolved out, or (iii) the single dish flux is erroneous, possibly because of confusion with galactic emission. However, the flux of the point sources seen in the GMRT images are in good agreement with those listed in NVSS, indicating that our calibration is not at fault. We note that in the case of KKH 12, KKH 6, UGC 6456, UGCA 92

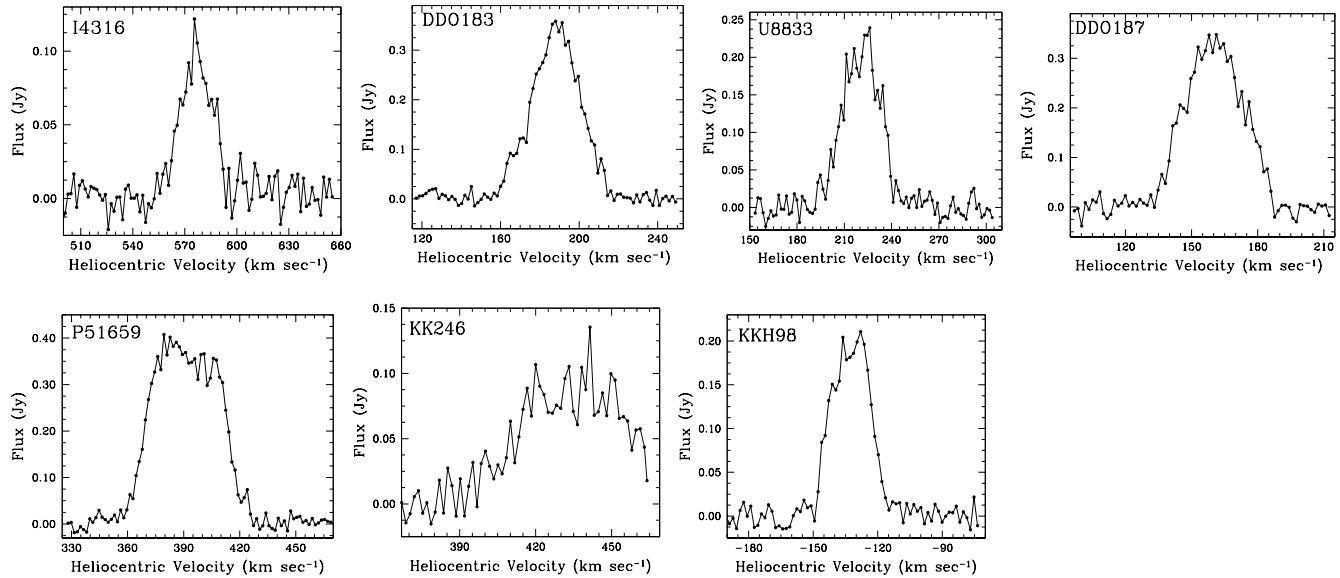


Figure 5. (continued) The global HI profiles of the sample galaxies obtained from the lowest resolution data cubes (see Table 2).

and KK 41 there is a strong local HI emission at velocities very close to the systemic velocities, making it likely that the single dish integrated flux measurements for these galaxies were contaminated by blending of their HI emission with that of the galactic emission. In the case of KK 246, its HI spectrum was near the edge of the GMRT observing band, hence the flux could not be reliably estimated.

The GMRT integrated HI emission of the sample galaxies, obtained from the coarsest resolution data cubes (see Table 2), overlaid on the optical Digitized Sky Survey (DSS) images are shown in Figure 6.

The HI morphological inclinations (i_{HI}) for our sample galaxies were estimated from the integrated HI maps by fitting elliptical annuli to the HI images at various resolutions. For sample galaxies which have HI disks less extended than 2 synthesised beams (across the diameter of the galaxy) at the lowest HI resolution, could in principle be derived from the higher resolution HI maps. However, for most sample galaxies ellipse fitting to the high resolution HI maps is not reliable because of clumpiness in the central high column density regions. The derived inclination (without applying any correction for the intrinsic thickness of the HI disk) is given in Column(10) in Table 3. Figure 7 shows a comparison between the morphological inclination derived from the optical and HI isophotes of the galaxy. No correction has been applied for the intrinsic thickness of the disk in both cases. The solid line shows a case when both inclinations are the same. We find that for 6 galaxies the HI inclination is significantly greater than the optical inclination (viz. KKH 11, UGC 6456, NGC 3741, UGC 8055, KK 230, KK 250). On the other hand, for many galaxies the optical inclination is found to be systematically higher than the inclination derived from the HI morphology. This result, if interpreted literally, suggest that the HI disks of these galaxies are thicker than the disks of their optical counterparts. However, we caution that a proper analysis using deconvolved angular sizes of the HI disks needs to be done before a firm conclusion can be drawn.

The diameter of the HI disk at a column density of

$N_{\text{HI}} \sim 10^{19}$ atoms cm^{-2} (except for UGCA 92 where the HI diameter is measured at $N_{\text{HI}} \sim 10^{20}$ atoms cm^{-2}) estimated from the lowest resolution integrated HI emission maps is given in Column(7) of Table 3. The ratio of the HI diameter to the optical (Holmberg) diameter for the sample is also given in Column(9) of the same table. Figure 8 shows the histogram of the derived HI extent of FIGGS at $N_{\text{HI}} \sim 10^{19}$ cm^{-2} , normalised to the Holmberg diameter of the galaxy. The median HI extent of the FIGGS sample (normalised to Holmberg diameter of the galaxy) is 2.4. For a comparison, Hunter (1997) using the data compiled from the literature for comparatively bright Im galaxies found that the ratio of $D_{\text{HI}}/D_{\text{Ho}}$ is somewhat smaller, viz. 1.5–2. The extreme outliers in Figure 8 is NGC 3741, our FIGGS data show it to have an HI extent of ~ 8.3 times D_{Ho} (Holmberg diameter). Follow-up WSRT+DRAO+GMRT observations resulted in HI being detected out to $\sim 8.8 D_{\text{Ho}}$ – NGC 3741 has the most extended HI disk known. For NGC 3741 the rotation curve could be derived out a record of ~ 44 times the disk scale length and from the last measured point of the rotation curve we estimate the dynamical mass to light ratio, $M_{\text{D}}/L_{\text{B}} \sim 149$ – which makes it one of the “darkest” irregular galaxies known (Begum et al. 2005, 2008).

Figure 9 shows a tight correlation between HI mass and the HI diameter, measured at N_{HI} of 1×10^{19} cm^{-2} for FIGGS sample. The galaxies in FIGGS sample with accurate distances are shown as solid points, whereas the remaining galaxies are shown as open circle. The best fit to the whole FIGGS sample shown as a solid line gives

$$\log(M_{\text{HI}}) = (1.99 \pm 0.11)\log(D_{\text{HI}}) + (6.08 \pm 0.06) \quad (1)$$

The best fit relation was also derived using only the galaxies with TRGB distances, however no significant difference was found between the best fit parameters derived in this case and that derived using the whole sample. Eqn.(1) implies that the HI disks of the FIGGS sample are well described as having a constant average surface mass density $\sim 1.5 M_{\odot} \text{pc}^{-2}$. A tight correlation between HI mass and the size of the HI disk has been noted

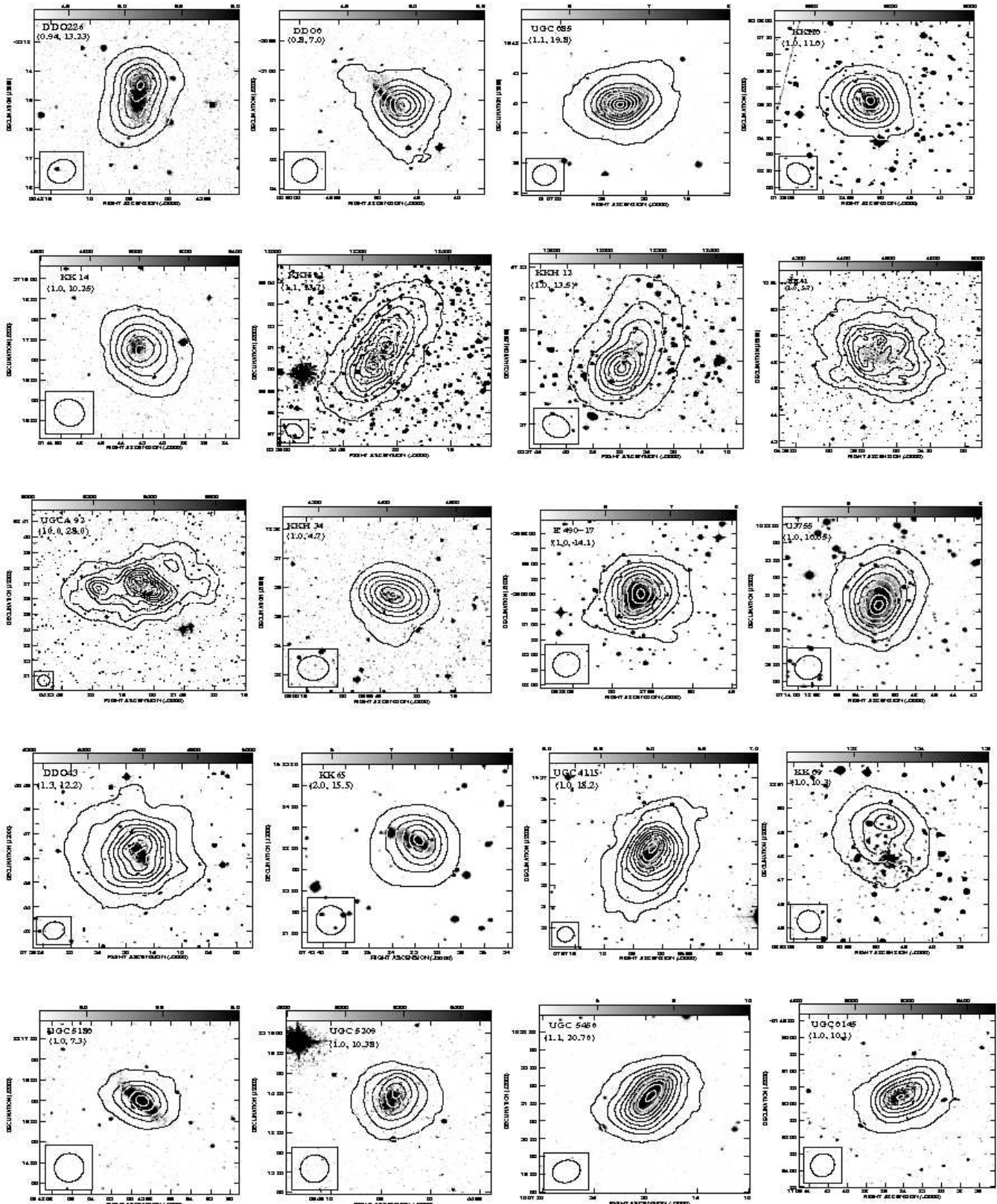


Figure 6. The GMRT integrated HI column density distribution (contours) overlaid on the optical DSS images (grey scales) of FIGGS galaxies from the lowest resolution data cubes (see Table 2). The contours are uniformly spaced. The first contour level and the contour separation are printed below the galaxy name in units of 10^{19} cm^{-2} .

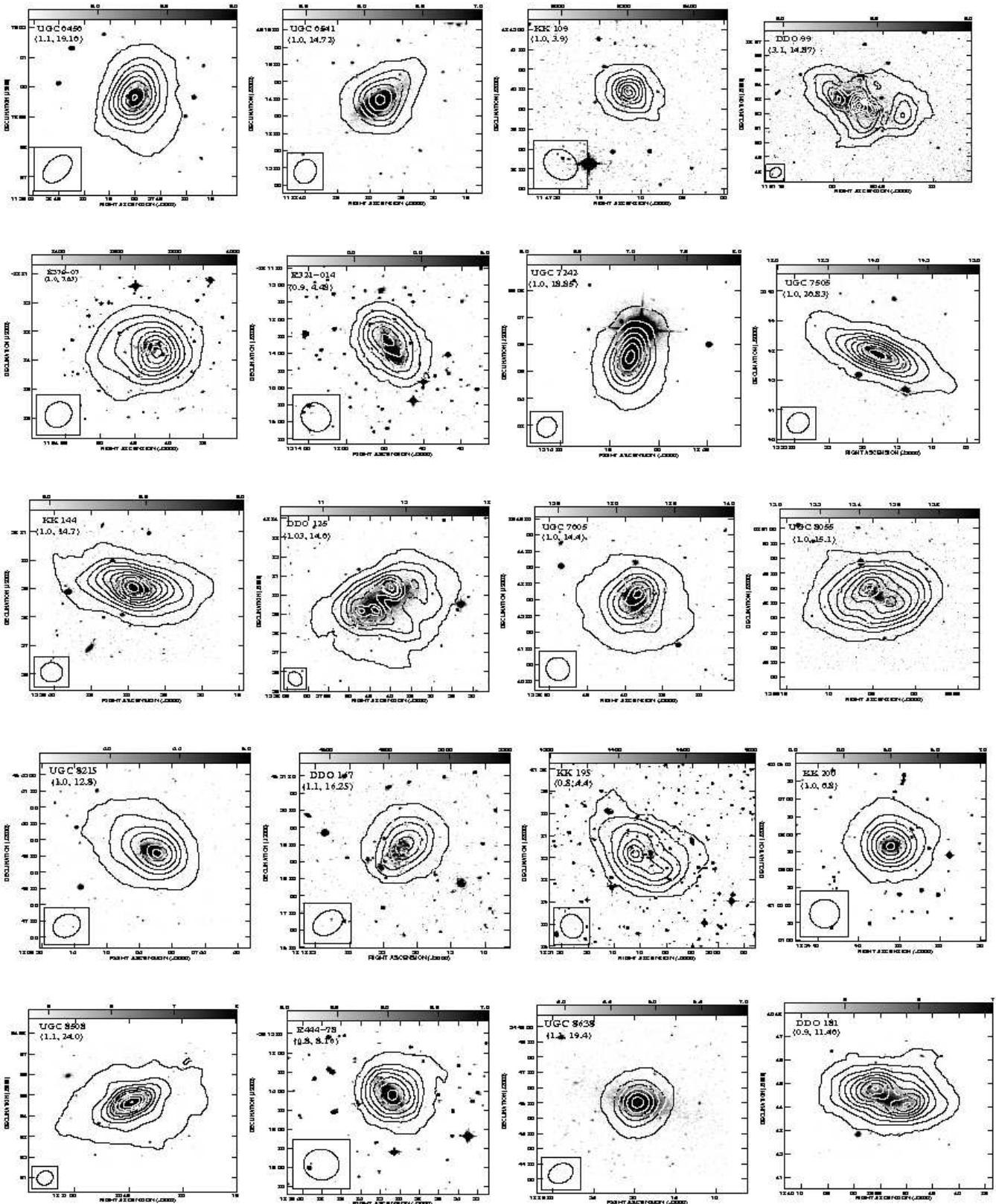


Figure 6. (continued) The GMRT integrated HI column density distribution (contours) overlaid on the optical DSS images (grey scales) of FIGGS galaxies from the lowest resolution data cubes (see Table 2). The first contour level and the contour separation are printed below the galaxy name in units of 10^{19} cm^{-2} .

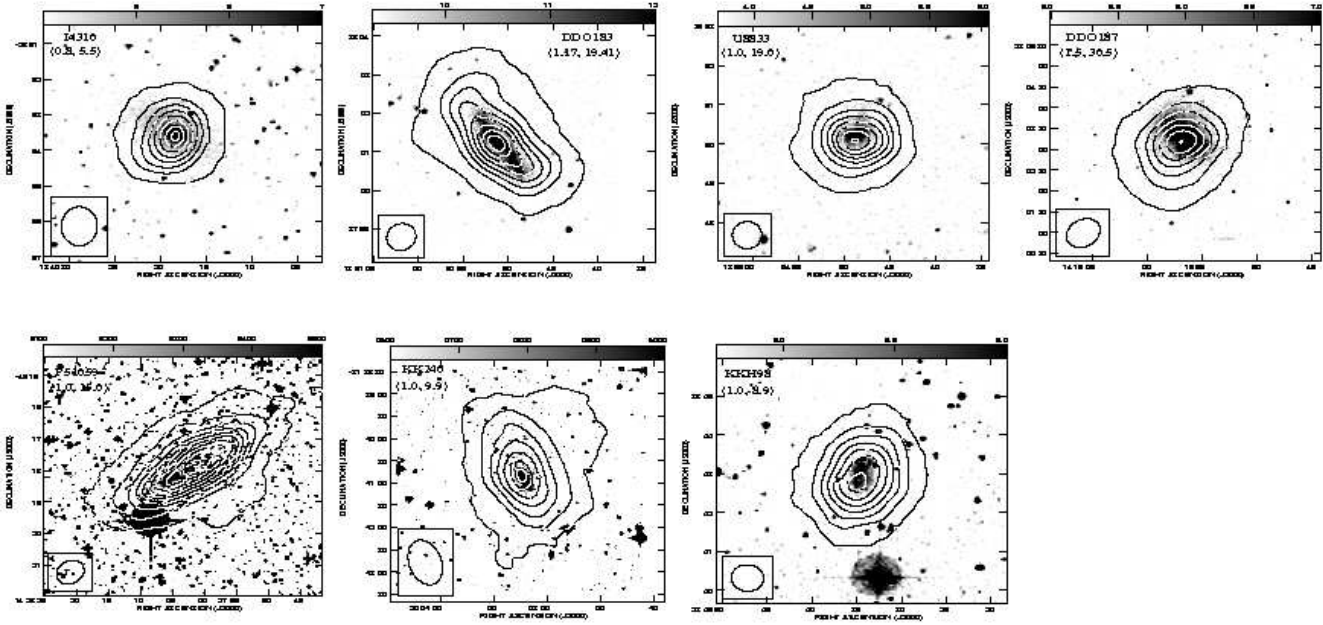


Figure 6. (continued) The GMRT integrated HI column density distribution (contours) overlaid on the optical DSS images (grey scales) of FIGGS galaxies from the lowest resolution data cubes (see Table 2). The first contour level and the contour separation are printed below the galaxy name in units of 10^{19} cm^{-2} .

earlier for spiral galaxies (e.g. Broeils & Rhee (1997)) and for brighter dwarf galaxies (Swaters 1999). For these samples the HI diameter was measured at a slightly higher column density, viz. $1 M_{\odot} \text{ pc}^{-2}$. For the FIGGS galaxies, the relationship between the HI mass and the HI diameter measured at $1 M_{\odot} \text{ pc}^{-2}$ is $\log(M_{\text{HI}}) = (1.96 \pm 0.10)\log(D_{\text{HI}}) + (6.37 \pm 0.07)$, for comparison, Broeils & Rhee (1997) measure $\log(M_{\text{HI}}) = (1.96 \pm 0.04)\log(D_{\text{HI}}) + (6.52 \pm 0.06)$. The fit coefficients overlap within the error bars. Hence from the FIGGS data we find that there is at best marginal evidence for a decrease in average HI surface density with decreasing HI mass; to a good approximation, the disks of gas rich galaxies, ranging over 3 orders of magnitudes in HI mass, can be described as being drawn from a family with constant HI surface density. The HI mass also correlates with the optical (Holmberg) diameter (shown in Fig. 10), although with a larger scatter. A linear fit with a slope and intercept of 1.74 ± 0.22 and 6.93 ± 0.18 , respectively is shown as a solid line. The larger scatter in the relation between M_{HI} and the optical diameter, also seen in sample of brighter dwarfs (e.g. Swaters (1999)), is probably indicative of a looser coupling between the gas and star formation in dwarfs, compared to that in spiral galaxies.

Figure 11 shows the HI mass to light ratio for the FIGGS sample plotted as a function of the HI extent, $D_{\text{HI}}/D_{\text{Ho}}$. A trend of an increase in the $M_{\text{HI}}/L_{\text{B}}$ with an increase in the HI extent of the galaxies is clearly seen. The best fit to the FIGGS sample shown as a solid line gives

$$\log\left(\frac{M_{\text{HI}}}{L_{\text{B}}}\right) = (1.31 \pm 0.18)\log\left(\frac{D_{\text{HI}}}{D_{\text{Ho}}}\right) + (-0.43 \pm 0.08) \quad (2)$$

van Zee et al.(1995) from a HI mapping of a sample of low luminosity galaxies also found an evidence of an extended HI extent for high $M_{\text{HI}}/L_{\text{B}}$ galaxies.

Figure 12 shows $M_{\text{HI}}/L_{\text{B}}$ for the FIGGS sample as a function

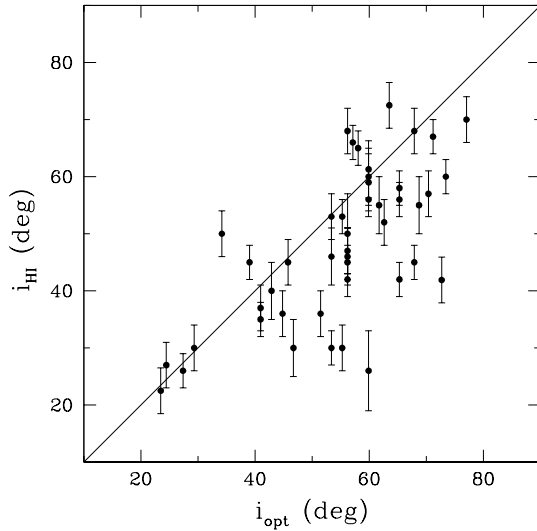


Figure 7. A comparison of the morphological optical and HI inclination of the FIGGS sample. The solid lines shows the case when the two inclinations are the same.

of M_{B} . The same quantity for several other spiral and dwarf galaxies, spanning a range in absolute B magnitude from $M_{\text{B}} \sim -23$ to $M_{\text{B}} \sim -9$ is also plotted. The sample from which these galaxies have been drawn are listed in the figure caption. The galaxies in FIGGS sample with TRGB distances are shown as solid circles, whereas the remaining FIGGS galaxies are shown as open circles. The solid line shows an empirically determined upper envelope for $M_{\text{HI}}/L_{\text{B}}$ as a function of a M_{B} from Warren et al. (2007). This upper envelope can be interpreted as a minimum fraction of the total

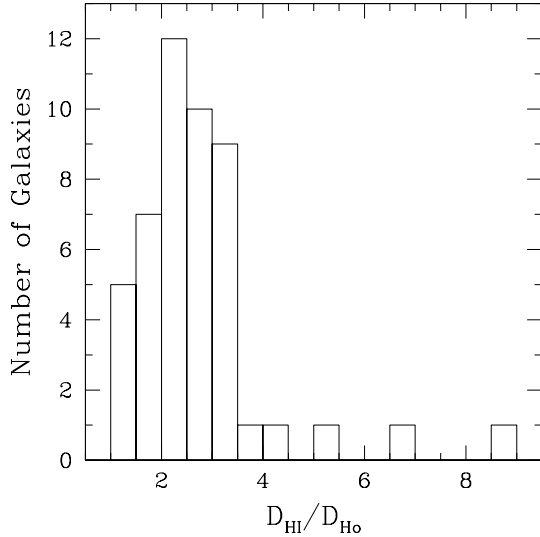


Figure 8. The histogram of the extent of the HI disk (measured at $N_{HI} = 1 \times 10^{19} \text{ cm}^{-2}$), normalised to the Holmberg diameter for the FIGGS sample.

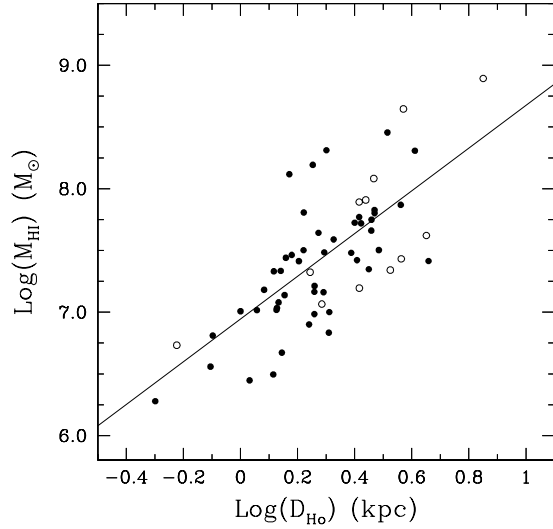


Figure 10. The HI mass for the FIGGS sample versus the Holmberg diameter. The solid line represents the fit to the data points. Galaxies in FIGGS sample with TRGB distances are shown as solid points, while the remaining galaxies in the sample are shown as open circles.

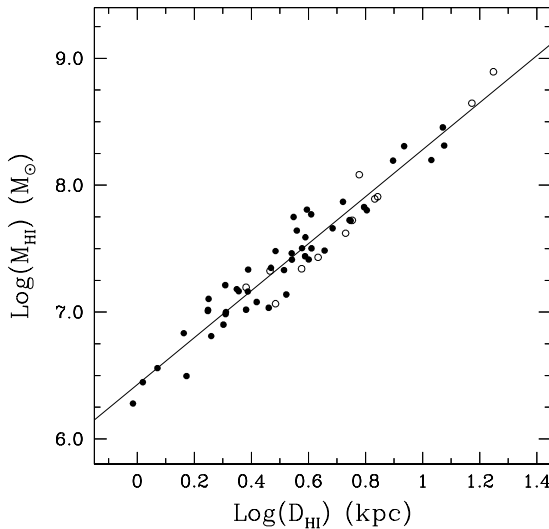


Figure 9. The HI mass for the FIGGS sample versus the HI diameter (measured at $N_{HI} \sim 10^{19} \text{ cm}^{-2}$). The solid line represents the fit to the data points. Galaxies in FIGGS sample with TRGB distances are shown as solid points, while the remaining galaxies in the sample are shown as open circles.

baryonic mass which needs to be converted into stars in order for a galaxy of a given baryonic mass to remain gravothermally stable (Warren et al. (2007)). It is interesting to note that except for And IV, all FIGGS galaxies lie much below this upper envelope. This implies that these galaxies have converted much more baryons into stars than the minimum required for remaining stable. In this context, it is interesting to note that the average gas fraction for the FIGGS sample is 0.7. Thus, for the majority of the dwarf galaxies in our sample, the baryonic mass is dominated by gas, rather than stars.

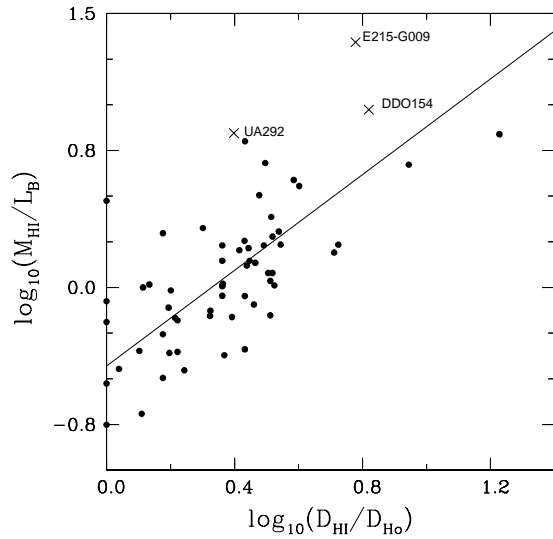


Figure 11. The log of HI mass to B band light ratio for the FIGGS sample plotted as a function of the extent of the HI disk (measured at $N_{HI} \sim 1 \times 10^{19} \text{ cm}^{-2}$) normalised to the Holmberg diameter. Crosses show three additional galaxies from the literature with high M_{HI}/L_B and extended HI disks, UA292 (Young et al. 2003), ESO215-G?009 (Warren et al. 2004) and DDO 154 (Carignan & Purton 1998).

In order to investigate the environmental dependence of the HI content for FIGGS galaxies, we plot M_{HI}/L_B for FIGGS sample as a function of tidal index (TI) (Figure 13). Some additional gas rich galaxies with known HI extent are also plotted in the figure. TI is taken from Karachentsev et al. (2004) and it represents the local mass density around a given galaxy, estimated using a large sample of galaxies within ~ 10 Mpc of the Milky Way. A negative value of TI for a galaxy indicates that the galaxy is isolated, whereas a pos-

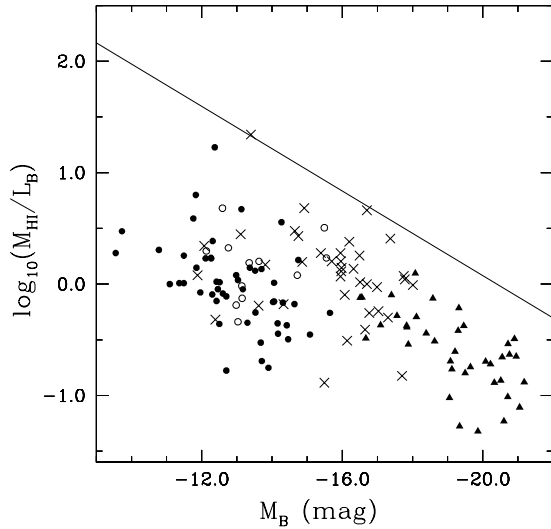


Figure 12. The log of HI mass to light ratio vs. B band absolute magnitude. Galaxies from FIGGS sample with TRGB distances are shown as solid points whereas the remaining FIGGS galaxies are shown as open circles. Crosses are galaxies from Warren et al.(2007) and solid triangles from Verheijen (2001). The solid line marks the locus of an upper envelope for the HI mass-to-light ratio at a given luminosity from Warren et al.(2007).

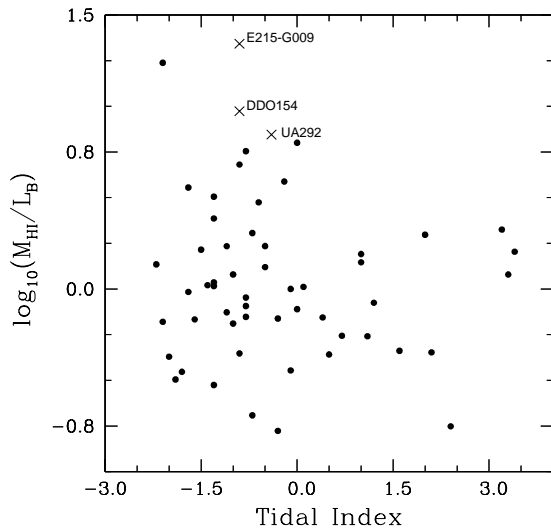


Figure 13. The log of HI mass to light ratio as a function of the tidal index for the FIGGS sample. Additional galaxies from literature with high $M_{\text{HI}}/L_{\text{B}}$ are also marked in the plot.

itive number indicates that the galaxy is in a dense environment. Figure 13. shows that most of the FIGGS galaxies are in less dense environments, and that all the galaxies with high $M_{\text{HI}}/L_{\text{B}}$ (i.e > 2.5) have negative tidal index i.e are isolated. Figure 14 shows the HI extent of the FIGGS sample, normalised to the optical (Holmberg) radius, plotted as a function of TI. As seen in the figure, the galaxies with very extended HI disks ($D_{\text{HI}}/D_{\text{Ho}} > 5.0$) are isolated.

To summarize, we have presented the first results from the

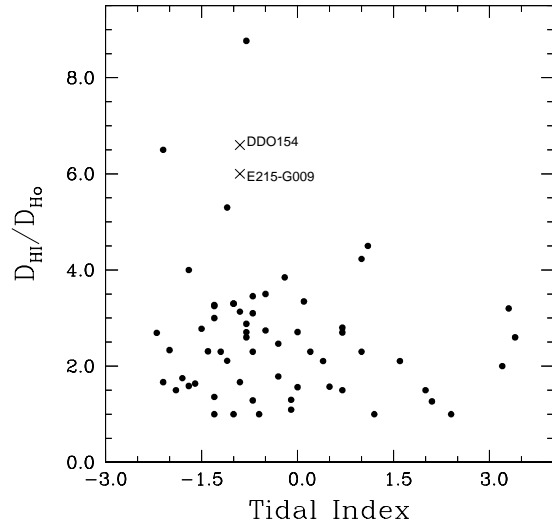


Figure 14. The HI extent of the FIGGS sample (normalised to the Holmberg radius) plotted as a function of the tidal index for the FIGGS sample. Additional galaxies from literature with very extended HI disks viz. DDO 154 and ESO215-G?009 and are also marked in the plot.

Faint Irregular Galaxies GMRT Survey (FIGGS). FIGGS is a large imaging program aimed at providing a comprehensive and statistically robust characterisation of the neutral ISM properties of extremely faint, nearby, gas rich, dIrr galaxies using the GMRT. The GMRT HI data is supplemented with observations at other wavelengths. The HI images in conjunction with the optical data will be used to investigate a variety of scientific questions including the star formation feedback on the neutral ISM, threshold for star formation, baryonic TF relation and dark matter distribution in low mass galaxies. The optical properties of the FIGGS sample, GMRT observations and the main science drivers for the survey are described. The GMRT integrated HI column density maps and the HI spectra for the sample galaxies are presented. The global HI properties of the FIGGS sample, derived from the GMRT observations, and their comparison with the optical properties of the sample galaxies are also presented. A detailed comparison of the gas distribution, kinematics and star formation in the sample galaxies will be presented in the companion papers.

ACKNOWLEDGMENTS

The observations presented in this paper were made with the Giant Metrewave Radio Telescope (GMRT). The GMRT is operated by the National Center for Radio Astrophysics of the Tata Institute of Fundamental Research. Partial support for this work was provided by ILTP grant B-3.13.

REFERENCES

- Begum, A., Chengalur, J.N. & Hopp, U., 2003, *New Astronomy*, 8, 267
- Begum, A & Chengalur, J.N., 2003, *A&A*, 409, 879
- Begum, A & Chengalur, J.N., 2004, *A&A*, 413, 525
- Begum, A & Chengalur, J.N., 2004, *A&A*, 424, 509
- Begum, A & Chengalur, J.N., 2005, *MNRAS*, 362, 609

- Begum, A, Chengalur, J.N. & Karachentsev, I. D., 2005, *A&A*, 433, 1L
- Begum, A, Chengalur, J.N., Karachentsev, I. D. & Sharina, M. E., 2005, *MNRAS*, 359, 53L
- Begum, A, Chengalur, J.N., Karachentsev, I. D., Kaisin, S. S. & Sharina, M. E., 2006, *MNRAS*, 365, 1220
- Begum, A, Chengalur, J.N., Kennicutt, R. C., Karachentsev, I. D. & Janice, L. C., 2008, *MNRAS*, 383, 809
- Bell, E. F., McIntosh, D. H., Katz, N. & Weinberg, M. D., 2003, *ApJSS*, 149, 289
- Blanton, M. R., Geha, M. & West, A. A. 2007 (*astro-ph/0707.3813*)
- Bouchard, A., Jerjen, H., Da Costa, G. S. & Ott, J., 2007, *AJ*, 133, 261
- Bremnes, T., Binggeli, B. & Prugniel, P., 1999, *A&AS*, 137, 337
- Bremnes, T., Binggeli, B. & Prugniel, P., 2000, *A&AS*, 141, 211
- Broeils, A. H. & Rhee, M. H., 1997, *A&A*, 324, 877
- Carignan, C., & Purton, C. 1998, *ApJ*, 506, 125
- Cannon, J. M., McClure-Griffiths, N. M., Skillman, Evan D. & Côté S., 2004, *ApJ*, 607, 274
- Corbin, M. R., Kim, H., Jansen, R. A., Windhorst, R. A. & Fernandes, R. C., 2008 *ApJ* (in press) (*astro-ph-0710.2557v1*)
- Cote, S., Freeman, K. C., Carignan, C. & Quinn, P. J., 1997, *AJ*, 114, 1313
- Côté S., Carignan, C. & Freeman, K. C., 2000, *AJ*, 120, 3027
- de Blok, W. J. G., Bosma, A. & McGaugh, S., 2003, *MNRAS*, 340, 657
- de Blok, W. J. G., 2005, *ApJ*, 634, 227
- Dekel, A. & Woo, J., 2003, *MNRAS*, 344, 1131
- Efstathiou, G. 2000, *MNRAS*, 317, 697
- Ekta, Chengalur, J. N., Pustilnik, S. A., 2006, *MNRAS*, 372, 853
- Ferguson, A. M. N., Gallagher, J. S. & Wyse, R. F. G., 2000, *AJ*, 120, 821
- Geha, M., Blanton, M. R., Masjedi, M. & West, A. A., 2006, *ApJ*, 653, 240
- Giovanelli, R. et al. 2005, *AJ*, 130, 2613
- Hoffman, G. L., Salpeter, E. E., Farhat, B., Roos, T., Williams, H. & Helou, G., 1996, *ApJS*, 105, 269
- Hopp, U. & Schulte-Ladbeck, R. E., 1995, *A&AS*, 111, 527
- Hunter, D., 1997, *PASP*, 109, 937
- Hunter, D. A. & Elmegreen, B. G., 2006, *ApJS*, 162, 49
- Huchtmeier, W. K. & Richter, O. G., 1986, *A&AS*, 63, 323
- Huchtmeier, W. K. & Skillman, E., 1998, *A&AS*, 127, 269
- Huchtmeier, W. K., Karachentsev, I. D. & Karachentseva, V. E., 2003 *A&A*, 401, 483
- Kanekar, N. & Chengalur, J. N., 2005, *A&A*, 429, L51
- Karachentseva I. D., Prugniel, P., Vennik, J., Richter, G. M., Thuan, T. X., & Martin, J. M., 1996, *A&AS*, 117, 343
- Karachentsev I. D., Makarova, L. N. & Andersen, M. I., 1999, *MNRAS*, 307, 37L
- Karachentsev I. D., Karachentseva V. E., Huchtmeier W. K. & Makarov D. I., 2004, *AJ*, 127, 2031
- Karachentsev I. D. et al., 2006, *AJ*, 131, 1361
- Kennicutt, R. C., 1989, *ApJ*, 344, 685
- Lo, K. Y., Sargent, W. L. W. & Young, K., 1993, *AJ*, 106, 507
- Makarova, L., 1999, *A&AS*, 139, 491
- Makarova, L., Karachentsev, I. D., Grebel, E. K. & Barsunova, O. Y., 2002, *A&A*, 384, 71
- Makarova, L., Karachentsev, I. D., Grebel, E. K., Harbeck, D., Korotkova, G. G. & Geisler, D., 2005, *A&A*, 433, 751
- McGaugh, S. S., Schombert, J. M., Bothun, G. D., de Blok, W. J. G., 2000, *ApJL*, 533, 99
- McGaugh, S. S., 2005, *ApJ*, 632, 859
- Mathews, L. D., Gallagher, J. S., Littleton, J. E., 1995, *AJ*, 110, 581
- Miralda-Escude, J. & Rees, M. J., 1997, *ApJ*, 478, 57
- Navarro et al., 2004, *MNRAS*, 349, 1039
- Parodi, B. R., Barazza, F. D. & Binggeli, B., 2002, *A&A*, 388, 29
- Pustilnik, S. A. & Martin, J. M., 2007, *A&A*, 464, 859
- Schaye, J., 2004, *ApJ*, 609, 667
- simon, J. D. & Geha, M., 2007, *ApJ*, 670, 313
- Simpson C. E., Hunter D. A., Nordgren T. E., 2005, *AJ*, 130, 1049
- Skillman, E. D., 1987, in *Star Formation in Galaxies*, edited by C. J. Lonsdale Persson, NASA, 263
- Springob, C. M., Haynes, M. P., Giovanelli, R. & Kent, B. R., 2005, *ApJS*, 160, 149
- Stil, J. M. & Israel. F. P., 2002, *A&A*, 389, 29
- Swarup, G., Ananthkrishnan, S., Kapahi, V.K., Rao, A.P., Subrahmanya, C.R. & Kulkarni, V.K. 1991, *Current Science*, 60, 95
- Swaters, R., 1999, PhD thesis, Rijksuniversiteit Groningen
- Taylor, C. L., Brinks, E., Pogge, R. W. & Skillman, E. D., 1994 *AJ*, 107, 971
- Taylor, V. A., Jansen, R. A., Windhorst, R. A., Odewahn, S. C. & Hibbard, J. E., 2005, *ApJ*, 630, 784
- Tully, B. et al. 2006, *AJ*, 132, 729
- van Zee, L., Haynes, M. P. & Giovanelli, R., 1995, *AJ*, 109, 990
- van Zee, L., 2000, *ApJ*, 119, 2757
- van den Bosch, F. C., Swaters, R. A., 2001, *MNRAS*, 325, 1017
- Verheijen, M.A.W & Sancisi, R., 2001, *A&A*, 370, 765
- Verheijen, M.A.W, 2001, *ApJ*, 563, 694
- Warren, B. E., Jerjen, H. & Koribalski, B. S., 2004, *AJ*, 128, 1152
- Warren, B. E., Jerjen, H. & Koribalski, B. S., 2007, *AJ*, 134, 1849
- Weldrake, D. T. F., de Blok, W. J. G. & Walter, F., 2003, *MNRAS*, 340, 12
- Young, L. M., van Zee, L., Lo, K. Y., Dohm-Palmer, R. C., & Beierle, M. E. 2003, *ApJ*, 592, 111
- Zwaan, M. A., Meyer, M. J., Stevely-Smith, L. & Webster, R. L., 2005, *MNRAS*, 359, L30